Manuscript prepared for J. Name
with version 5.0 of the LaTeX class copernicus.cls.
Date: 12 September 2014

Fast transport from Southeast Asia boundary layer sources to Northern Europe: rapid uplift in typhoons and eastward eddy shedding of the Asian monsoon anticyclone

B. Vogel[1], G. Günther[1], R. Müller[1], J.-U. Grooß[1], P. Hoor[2], M. Krämer[1], S. Müller[2], A. Zahn[3], and M. Riese[1]

[1]Forschungszentrum Jülich, Institute of Energy and Climate Research – Stratosphere (IEK-7), Jülich, Germany
[2]Institute for Atmospheric Physics, University of Mainz, Mainz, Germany
[3]Institute for Meteorology and Climate Research, Karlsruhe Institute of Technology, Karlsruhe, Germany

Correspondence to: B. Vogel (b.vogel@fz-juelich.de)

Abstract. ~~During the TACTS aircraft campaign enhanced~~ Enhanced tropospheric trace gases such as CO, CH_4, and H_2O and reduced stratospheric O_3 were measured in situ in the lowermost stratosphere over Northern Europe on 26 September ~~2012.~~ 2012 during the TACTS aircraft campaign. The measurements indicate that these air masses clearly differ from the stratospheric background. The calculation of 40 day backward trajectories with the trajectory module of the CLaMS model shows that these air masses are affected by the Asian monsoon anticyclone. Some air masses originate from the boundary layer in Southeast Asia/West Pacific and are rapidly lifted (1–2 days) within a typhoon ~~.~~ ~~Afterwards they are injected directly into~~ up to the outer edge the Asian monsoon anticyclone. Afterwards the air parcels are entrained by the anticyclonic circulation of the Asian monsoon. The subsequent long-range transport (8–14 days) of enhanced water vapour and pollutants to the lowermost stratosphere in Northern Europe is driven by eastward transport of tropospheric air from the Asian monsoon anticyclone caused by an eddy shedding event. We find that the combination of rapid uplift by a typhoon and eastward eddy shedding from the Asian monsoon anticyclone is ~~an additional~~ a novel fast transport pathway that ~~, in this study, carries~~ may carry boundary emissions from Southeast Asia/West Pacific within approximately 5 weeks to the lowermost stratosphere in Northern Europe.

1 Introduction

One of the most pronounced circulation patterns in the the upper troposphere and lower stratosphere (UTLS) during boreal summer is the Asian summer monsoon circulation. It consists of a large-scale anticyclone in the UTLS extending from Asia to the Middle East from early June until end of September. The Asian monsoon anticyclone extends into the lowermost stratosphere (e.g., Randel and Park, 2006), where the tropopause above the monsoon is higher than in the extratropics by about 50 K (e.g., Dunkerton, 1995; Highwood and Hoskins, 1998). The anticyclone is flanked by an equatorial easterly jet to the south and by the subtropical westerly jet to the north and is characterised by low values of Potential Vorticity (PV) (e.g., Randel and Park, 2006).

In general, the Asian monsoon circulation provides an effective pathway for water vapour (Ploeger et al., 2013) and pollutants to the lower stratosphere of the Northern Hemisphere. Water vapour (H_2O) is the most important greenhouse gas and moistening of the stratosphere is an important driver of climate change (e.g., Forster and Shine, 1999, 2002; Shindell, 2001; Smith et al., 2001; Vogel et al., 2012). In particular, even small changes of H_2O in the UTLS have an impact on surface climate (e.g., Solomon et al., 2010; Riese et al., 2012). In spite of its radiative importance changes and trends in UTLS water vapour are only poorly quantified (e.g., Hurst et al., 2011; Kunz et al., 2013). ~~Further~~Furthermore, increasing amounts of the greenhouse gas methane (CH_4) ~~, in addition,~~ enhance stratospheric water vapour concentrations by methane oxidation (e.g., Röckmann et al., 2004; Riese et al., 2006; Rohs et al., 2006). Methane emissions by rice paddies in India and Southeast Asia (e.g., Khalil et al., 1998; Huang et al., 2004) may provide an important contribution to stratospheric CH_4 in this context. Enhanced water vapour concentrations in the UTLS affect not only the radiative balance, but have also the potential to af-

fect stratospheric chemistry (e.g., Kirk-Davidoff et al., 1999; Dvortsov and Solomon, 2001; Vogel et al., 2011a). An increasing population and growing industries in Asia along with climate change have the potential to enhance future entry concentrations of water vapour and pollutants into the stratosphere ~~caused~~ transported by the Asian monsoon anticyclone. Therefore it is important to identify transport pathways to the global stratosphere to allow potential environmental risks to be assessed.

The Asian summer monsoon is associated with strong upward transport of tropospheric source gases by deep convection which is confined by the strong anticyclonic circulation (e.g., Li et al., 2005; Randel and Park, 2006; Park et al., 2007, 2008, 2009). Hence, in satellite measurements relatively large concentrations of tropospheric trace gases such as water vapour (H_2O) (Rosenlof et al., 1997; Jackson et al., 1998), carbon monoxide (CO) (Li et al., 2005; Park et al., 2008), and methane (CH_4) (Park et al., 2004; Xiong et al., 2009) are found in the Asian monsoon anticyclone, isolated by a transport barrier from the surrounding air. ~~Vice versa~~ Conversely stratospheric trace gases such as O_3 show low concentrations in the anticyclone (Randel and Park, 2006; Liu et al., 2009; Konopka et al., 2010). However, the impact of different boundary layer sources on the chemical composition of the air in the Asian monsoon anticyclone (e.g., Li et al., 2005; Park et al., 2009; Chen et al., 2012; Bergman et al., 2013) and the mechanisms for transport into the lowermost stratosphere (Dethof et al., 1999; Park et al., 2009; Randel et al., 2010; Bourassa et al., 2012) are subject of current debate.

Trajectory calculations suggest air mass contributions in the Asian monsoon anticyclone from boundary sources originating in India/Southeast Asia (including the Bay of Bengal) and the Tibetan Plateau (Chen et al., 2012; Bergman et al., 2013). Chen et al. (2012) found the main contribution to air at tropopause height from the tropical Western Pacific region and the South China Seas, while Bergman et al. (2013) found that contributions from the Tibetan Plateau are most important at 100 hPa. In the Asian monsoon, findings by Chen et al. (2012) indicate that timescales of transport from the boundary layer to the tropopause region by deep convection overshooting are about 1–2 days, while several weeks by large scale ascent. Further, there is evidence that emissions on the eastern side of the anticyclone (northeast India and southwest China) are lifted upward and trapped in the Asian monsoon anticyclone (Li et al., 2005).

There is evidence that the mean upward transport at the eastern/southeastern side of the Asian monsoon anticyclone is a gateway of tropospheric air to the stratosphere by direct convective injection (Rosenlof et al., 1997; Park et al., 2007, 2008; Chen et al., 2012). However, the impact of this effect on the composition of the stratosphere has not been isolated from the influence of the transport in the deep tropics, entrained into the upward Brewer–Dobson circulation (Gettelman et al., 2004; Bannister et al., 2004), which is the primary transport pathway of air from the troposphere to the stratosphere (Holton et al., 1995).

One of the possible pathways for long-range transport of air masses from the Asian monsoon anticyclone to the extratropical lowermost stratosphere are smaller anticyclones breaking off a few times each summer from the main anticyclone characterised by low PV values (Hsu and Plumb, 2001; Popovic and Plumb, 2001; Garny and Randel, 2013). This process is referred to as "eddy shedding". Westward transport of monsoon air masses by eddy shedding from the Asian monsoon anticyclone seems to be a common phenomenon, in contrast to eastward migrating anticyclones that occur less frequently (Popovic and Plumb, 2001; Garny and Randel, 2013). Garny and Randel (2013) found that westward propagation often ~~appear~~ appears after periods of strong convective forcing. Hsu and Plumb (2001) inferred from shallow-water calculations that~~in case~~, if the anticyclone is sufficiently ~~large~~ asymmetric, the elongated anticyclone becomes unstable and westward eddy shedding ~~occurred~~occurs. In contrast, eastward eddy shedding is ascribed to the interaction of the monsoon anticyclone with an eastward moving mid-latitude synoptic-scale tropospheric cyclone (Dethof et al., 1999).

Eddy shedding events have the potential to carry air with ~~enhanced~~ tropospheric trace gases such as water vapour or pollutants from the Asian monsoon anticyclone to mid and high latitudes of the Northern Hemisphere (Dethof et al., 1999; Garny and Randel, 2013). These air masses can be transported into the extratropical lower stratosphere where they are eventually mixed irreversibly with the surrounding stratospheric air (Dethof et al., 1999; Garny and Randel, 2013) and thus affect the chemical and radiative balance of the extra-tropical UTLS.

In this paper, we show that fast transport from boundary emissions from Southeast Asia has the potential to affect the chemical composition of the lowermost stratosphere over Northern Europe. We focus on the question how transport pathways and time scales from surface emissions from Southeast Asia are influenced by the Asian monsoon circulation and its interaction with tropospheric weather systems.

We use in situ measurements obtained during the TACTS (Transport and Composition in the Upper Troposphere and Lowermost Stratosphere) aircraft campaign 2012 and Lagrangian backward trajectories calculated with the trajectory module of the Chemical Lagrangian Model of the Stratosphere (CLaMS) (e.g., McKenna et al., 2002a,b; Konopka et al., 2010, and references therein). Pure trajectory models represent the advective transport by the resolved flow using three-dimensional winds from meteorological data sets and are therefore useful for investigating of the origin of air masses, in particular in the region of the Asian monsoon anticyclone (Dethof et al., 1999; Chen et al., 2012; Bergman et al., 2013). The paper is organised as follows: Sect. 2 describes the measurements and Sect. 3 the trajectory calculations. In Sect. 4, the interaction of tropospheric weather systems, in particular of typhoons, with the Asian monsoon

anticyclone and the resulting impact on the behaviour of the backward trajectories is ~~discussed. A~~presented. Our findings are discussed in Sect. 5 followed by a short summary and ~~conclusion are given~~ conclusions in Sect. ~~5.~~ 6.

2 Measurements of enhanced tropospheric trace gases in the stratosphere over Northern Europe

We use in situ measurements obtained during the TACTS aircraft campaign in August and September 2012. The TACTS campaign was designed to study Transport and Composition in the Upper Troposphere and Lowermost Stratosphere. It was conducted jointly with the ESMVal (Earth System Model Validation) measurement campaign. Both TACTS and ESMVal were performed using the German High Altitude and LOng Range Research Aircraft HALO, a Gulfstream V.

Here, we focus on the last research flight performed during TACTS/ESMVal on 26 September 2012 based out of Special Airport Oberpfaffenhofen (near Munich, 48° N 11° E), Germany. The flightpath is shown in Fig. 1 in conjunction with PV at 375 K potential temperature. ~~The flight~~ PV is based on ERA-Interim reanalysis data (Dee et al., 2011) (see Sect. 3). The aircraft was flown roughly to the west to the British Isles, then to the north to the Atlantic Ocean, thereafter to the east towards Scandinavia. A closed loop flight track (hexagon) was conducted over Norway to test the capability of the newly developed Gimballed Limb Observer for Radiance Imaging of the Atmosphere (GLORIA) to sound the atmosphere tomographically (Kaufmann et al., 2014; Riese et al., 2014). Thereafter, a flight pattern with a steep descent to the lower troposphere and directly afterwards a ~~step~~ steep ascent back to the stratosphere (referred to as "dive") was flown inside the hexagon. The research flight ended in Oberpfaffenhofen.

In this work, measurements of the following in situ instruments are used:

- The measurements of CO and CH_4 during TACTS/ESMVal were made with the TRIHOP instrument, which is an updated version of the three-channel tunable diode laser instrument for atmospheric research (TRISTAR), which has been used during the SPURT[1] project (Hoor et al., 2004; Engel et al., 2006). During the flight on 26 September 2012, TRIHOP achieves a precision of 0.9 ppbv for CO and ~~5~~10 ppbv for CH_4 ~~, respectively,~~ for 1.5 s integration time. ~~We estimate the reproducibility during the flights was~~ From the standard deviation of the in-situ calibrations, which were performed every 20 minutes, we estimate a reproducibility of the calibrations of 2.3 ppbv for CO and 15 ppbv for CH_4 ~~, respectively,~~ without any corrections applied. The reproducibility can be regarded as an upper limit for the drift of the measurements between the calibrations.

- The water measurements on board the HALO aircraft were obtained by the Fast In-situ Stratospheric Hygrometer (FISH) which is based on the Lyman-α photofragment fluorescence technique. Instrument and calibration procedure are described in Zöger et al. (1999). The FISH inlet is mounted forward-facing thus measuring total water, i.e. the sum of gas-phase water and water in ice particles. The procedure to correct the data for oversampling of ice particles in the forward-facing inlet is discussed in Schiller et al. (2008).

- A light-weight (14.5 kg) instrument (named FAIRO) for measuring ozone (O_3) with high accuracy (2 %) and high time resolution (10 Hz) was developed for the use on board HALO. It combines a dual-beam UV photometer with an UV-LED as light source and a dry chemiluminescence detector (Zahn et al., 2012). The performance of FAIRO was excellent during all 13 flights during TACTS/ESMVAL.

- Potential temperature is deduced from the Basic Halo Measurement and Sensor System (BAHAMAS) which yield basic meteorological and avionic data of HALO.

Figure 2 shows potential temperature (top, black dots) at the measurement location, CO and O_3 (middle), and CH_4 and H_2O (bottom) along the flightpath of the flight on 26 September 2012. In the first half of the flight at altitudes between 370 K and 380 K potential temperature, enhanced concentrations of tropospheric trace gases CO, CH_4, and H_2O were measured in the lowermost stratosphere and also reduced values of the stratospheric trace gas O_3. In Fig. 2, the time period from 09:05 UTC (Universal Time Coordinated) to 10:17 UTC with enhanced tropospheric trace gases and reduced ozone ~~, respectively,~~ is shaded in grey. Strong gradients are found in tracer measurements (at the beginning and the end of this time period) at the same level of potential temperature indicating that air masses were sampled with strongly different origin compared to the background air probed in this part of the flight. The region showing the enhanced tropospheric trace gases is referred to as "region of interest". The region of interest is located at the northwestern flank of the flight path over the Atlantic Ocean as shown in Fig. 1 (shown as white line in the flightpath). The potential vorticity (PV) at 375 K potential temperature indicates that in the region of interest and in the hexagon lower values of PV (7.3–8.0 PVU, yellow in Fig. 1) occur than in the stratospheric background, corroborating that these air masses have a different origin, that is more tropospheric, compared to the background. This is also evident in the Fig. 2 ~~, where~~where, within the flight part conducted within the hexagon shortly before the dive (≈ 13:00 UTC)~~conducted within the hexagon~~ , enhanced CO, CH_4, and H_2O and

[1] SPURenstofftransport in der Tropopausenregion (SPURT)

reduced O_3 ~~was~~ were measured simultaneously. Between 08:05 UTC and 08:23 UTC a tropospheric signal is also evident in the observations (see Fig. 2) measured over the British Isles (Fig. 1). However, in the region of interest the measured signatures are most pronounced and therefore we focus here on that part of the flight.

3 Results of backward trajectory calculations

To study the origin of air in the region of interest (highlighted in grey in Fig. 2) 40 day backward trajectories are calculated along the flightpath using wind data from the ERA-Interim ~~re-analysis~~ reanalysis (Dee et al., 2011) (with a horizontal resolution of $1° \times 1°$) provided by the European Centre for Medium-Range Weather Forecasts (ECMWF). For trajectory calculations, the trajectory module of the Chemical Lagrangian Model of the Stratosphere (CLaMS) (McKenna et al., 2002b; Konopka et al., 2012, and references therein) is used. Trajectory calculations with CLaMS can be performed in both the diabatic mode and the kinematic mode, i.e. using potential temperature or pressure, respectively, as the vertical coordinate (Ploeger et al., 2010). Here, the diabatic approach is applied ~~. This implies~~ using the diabatic heating rate (with contributions from radiative heating including the effects of clouds, latent heat release, mixing and diffusion) as vertical velocity including the daily cycle (more details see Ploeger et al., 2010). The transport is simulated with vertical velocities from the diabatic heating rate in the UTLS (< 300 hPa) and using a pressure based hybrid vertical coordinate in the troposphere (> 300 hPa) (Pommrich et al., 2014).

40 day backward trajectories starting at the observation along the flight path (every 10 s) on 26 September 2012 and ending at the origin of the air masses in the past (17 August 2012) are calculated (in total 3582 trajectories). The potential temperature at the air mass origin (Θ_{org}) gives information about the vertical transport of the air mass along the trajectory. In Fig. 2 (top), the potential temperature at the air mass origin (Θ_{org}) is shown as red dots. Most Θ_{org} values lie above or at the same level of potential temperature as during the flight, consistent with the descent of air masses in the lower stratosphere of the Northern Hemisphere. However, in the region of interest (432 trajectories) some of the air masses originate at much lower levels of potential temperature, namely between 295 K and 360 K.

In Fig. 3, ~~two~~ trajectories from two different Θ_{org} intervals, 295–320 K (left) and 320–360 K (right), are shown colour-coded by potential temperature (top) and by days reversed from 26 September 2012 (middle). Further, the geographical air mass origin (bottom, red dots in embedded map) and potential temperature vs. time along the 40 day backward trajectories (bottom) colour-coded by latitude are shown.

All air parcels with Θ_{org} below 360 K are affected by air masses originating from the Asian monsoon anticyclone (Fig. 3, top). The air parcels are separated from the Asian monsoon circulation in the region over Japan, East China, and Southeast Siberia approximately 8–14 days before they were sampled during the flight on 26 September 2012 (Fig. 3, middle).

Air masses ~~with Θ_{org} lower than 320K originate~~ originating at much lower levels of potential temperature ~~and~~ , below 320 K ($\Theta_{org} < 320$ K), are lifted between 35 and 40 days before the flight over the West Pacific (Fig. 3, left middle). Afterwards, they move first anti-clockwise at the edge of the anticyclone (at ≈ 365 K), then turn over Japan before they become entrained into the Asian monsoon circulation and then move further around the Asian monsoon (left middle). For Θ_{org} between 320 K and 360 K, some of the air masses intrude directly into the anticyclone and move clockwise round the Asian monsoon at the edge of the anticyclonic circulation. Other trajectories perform first a loop over the West Pacific ocean (right middle).

Some of the air parcels with Θ_{org} lower than 320 K show a very rapid uplift between 23 and 25 August with a maximum ascent rate of 41 $\mathrm{K\,day^{-1}}$ ($= 523\,\mathrm{hPa\,day^{-1}}$) and originate in Southeast Asia (left bottom). Air parcels with Θ_{org} between 320 K and 360 K are characterised by rapid uplift up to 13 $\mathrm{K\,day^{-1}}$ ($= 139\,\mathrm{hPa\,day^{-1}}$) between 18 and 24 August and originate in the West Pacific (northern or western of Philippines) or from northern of India (right bottom). An overview about maximum and mean vertical velocities is given in Table 1.

In the following we discuss also transport pathways of air masses originate in higher levels of potential temperature, namely in intervals for Θ_{org} between 360–370 K, 370–380 K, and 380–420 K. ~~Related figures are not shown here, but are available as an electronic supplement of this paper.~~

Most air masses originating at Θ_{org} values between 360 K and 370 K experienced a moderately rapid uplift with mean values of about 2 $\mathrm{K\,day^{-1}}$ ($= 22\,\mathrm{hPa\,day^{-1}}$) roughly in the region of the Asian monsoon anticyclone. Most of these air masses originate in North Africa, South Asia, and in the West Pacific (see Fig. 4 (top)). The trajectories are separated from the anticyclone approximately 8–14 days before the flight on 26 September 2012, and therefore transport air masses from inside the Asian monsoon anticyclone to Northern Europe (shown in Fig. 1 left in the electronic supplement of this paper).

At levels above, for Θ_{org} between 370 K and 380 K, the trajectories are affected by both the Asian monsoon anticyclone and the subtropical westerly jet. The moderate uplift along the trajectories is 1 $\mathrm{K\,day^{-1}}$ ($= 16\,\mathrm{hPa\,day^{-1}}$) in the mean. The majority of air masses originate in regions around the Asian monsoon anticyclone and in Central America (see Fig. 4 (middle)). In the latter case, the trajectories are most likely affected by the North American monsoon (shown in Fig. 1 right in the electronic supplement of this paper).

Most air masses that originate at Θ_{org} between 380 K and 420 K are dominated by the global circulation patterns with a descent of air masses in the Northern Hemisphere lower

stratosphere. These trajectories do not circulate around the Asian monsoon anticyclone (except for two trajectories) and the air mass origins are spread out in the entire Northern Hemisphere, excluding regions affected by the Asian monsoon anticyclone such as South Asia or parts of North Africa (see Fig. 4 (bottom) and Fig. 2 in the electronic supplement of this paper). Our findings inferred from backward trajectory calculations are summarised in Table 1.

Our trajectory calculations suggest that ~~potential~~ air masses from altitudes, which are potentially strongly affected by boundary emissions from Southeast Asia and the West Pacific, are rapidly uplifted and are transported within approximately 5 weeks to Northern Europe. The air mass origins are not found in surface regions located closed to the core of the Asian monsoon such as North India, South India or East China. This suggests that ~~in our study possible~~ boundary emissions from these regions ~~need a~~ may need a longer time period ~~of~~ for upward transport within the Asian monsoon anticyclone to reach the lowermost stratosphere over Northern Europe. However, we cannot rule out that a strong uplift in convection over India and Tibet is not well enough resolved in ERA-Interim reanalysis data.

In this work, we focus on the region of interest (cf. Sect. 2), however also in other parts of the flight enhanced tropospheric signals in tracers and reduced ozone are measured between 08:05 UTC and 08:23 UTC and along the hexagon before the dive. The latter signal is also caused by transport of air masses from lower levels of potential temperature as evident in 40 day backward trajectories (Fig. 3, top). The tropospheric signal between 08:05 UTC and 08:23 UTC is not present in 40 day backward trajectories, but ~~in 50~~is evident in 60 day backward trajectories ~~to a small extend. The trajectories from lower levels originate in South Asia, Northwest America and over the Atlantic ocean~~as discussed in Sect. 5.3.

4 Interaction between the Asian monsoon anticyclone and other tropospheric weather systems

To understand the behaviour of the backward trajectories presented in the previous section, the meteorology of the Asian monsoon area will be analysed based on ERA-Interim ~~re-analysis~~ reanalysis data (Dee et al., 2011). In August 2012, the Asian monsoon anticyclone was well established over Southern Asia and the Middle East. The Asian monsoon anticyclone is characterised by low PV values, indicating that it consists mainly of air masses of tropospheric origin. To the north the Asian monsoon anticyclone is connected to the subtropical jet, to the south the equatorial westward flow is adjacent. The Asian monsoon anticyclone extends over a height range from 400 hPa or 340 K upward well into the lowermost stratosphere.

During August and September 2012 several tropical cyclones had impact on meteorological conditions in the vicinity of the Asian monsoon anticyclone. Further, during September 2012 the subtropical jet over Asia was disturbed by strong Rossby waves triggered by low pressure systems travelling with the Arctic jet. The interaction between these disturbances and the Asian monsoon anticyclone is discussed in the next sections.

4.1 Very rapid uplift in tropical cyclones in August 2012

In the northwestern Pacific region, tropical cyclones (typhoons) are observed at all times of the year, with storm activity peaking in late northern summer (e.g., Emanuel, 2003). In August and September 2012, several major typhoons of the category 4 or 5 according to the Saffir–Simpson hurricane wind scale (SSHWS) occurred in the northwestern Pacific region.

Between 18 and 20 August 2012, the typhoon Tembin (named Igme by the Philippine Atmospheric, Geophysical and Astronomical Services Administration PAGASA) grew from a tropical depression to a category 4 typhoon southeast of Taiwan[2]. Only a few days later the tropical typhoon Bolaven (PAGASA name Julian) formed east of the Philippines and moved northwest towards Taiwan. Bolaven was also classified as a class 4 typhoon[3]. After having made landfall twice in Taiwan, Tembin started to interact with Bolaven on 25 August, forcing ~~it~~ Bolaven to move further to the north, where it made landfall in Korea on 28 August. Two days later, Tembin made landfall in Korea as well.

Figure 5 (top) shows the geographical position of the typhoons Tembin and Bolaven on 24 August 2012. Tembin was located over Taiwan, Bolaven further to the east over the Philippine Sea, being much stronger than Tembin at that time. The position of Bolaven coincides in time and space with the very rapid uplift of air masses evident in the trajectory calculations for Θ_{org} between 295 K and 320 K on 23/24 August 2012 (see Fig. 3, bottom).

Figure 5 (bottom) shows that both typhoons lifted air masses rapidly from the lower troposphere up to the tropopause region. The maximum updraft in a typhoon occurs at the eyewall, a ring of very deep convective clouds extending from the outer edge of the eye outward another 20–50 km (Emanuel, 2003). Maximum vertical uplift up to 300 hPa within 6 h ($0.014\,\mathrm{hPa\,s^{-1}}$) is found at around 135° E at the eastern flank of Bolaven. This very rapid vertical transport is consistent with upward motion calculated along the 40 day backward trajectories of up to $276\,\mathrm{hPa/6\,h}$ (see Table 1).

Bolaven moved northward during the next 4 days until it made landfall in Korea. This motion is also visible in the 40 day backward trajectories for Θ_{org} between 295 K and 310 K. Along the trajectories the air parcels move

[2] see e.g., http://www.nasa.gov/mission_pages/hurricanes/archives/2012/h2012_Tembin.html

[3] see e.g., http://www.nasa.gov/mission_pages/hurricanes/archives/2012/h2012_Bolaven.html

first cyclonically around the typhoon, before they move northward and enter the outer edge of the anticyclonic flow of the Asian monsoon anticyclone over Korea at ≈ 370 K (see Fig. 3 left middle panel).

For our trajectory calculations ERA-Interim reanalysis data are used. In ERA-Interim reanalysis data changes are implemented to improve deep and mid-level convection compared to previous reanalysis data (Dee et al., 2011), however small-scale rapid uplift in convective cores is not included. To show that the uplift in typhoons as represented in the ERA-Interim reanalysis data is strong enough to transport air parcels from the boundary layer to the Asian monsoon anticyclone as found in our backward trajectory calculations, we calculated forward trajectories starting in the boundary layer around the position the typhoon Bolaven on 23 August 2012 12:00 UTC (in a window of 15°N-25°N, 128°E-140°E and below $\approx$ 310 K potential temperature). The trajectories are started at a horizontal grid of 0.5° $\times$ 0.5° and a vertical grid of 1 K. Within 48 hours (23-25 August 2012 12:00 UTC), 10 % of these trajectories experience a strong uplift greater than 50 K potential temperature as shown in Fig 6. This very rapid uplift is also found on other days (22-26 August 2012) for both Bolaven and Tembin (not shown here). These calculations demonstrate that trajectories based on ERA-Interim reanalysis data show very rapid uplift and can reach the lower stratosphere, in spite of the fact that ERA-Interim reanalysis data do not resolve small-scale rapid uplift in convective cores. Therefore, the ERA-Interim reanalysis data are well suited to identify transport pathways from the boundary layer in Asia to the lowermost stratosphere over Northern Europe. We expect that in data sets including in addition the small-scale rapid uplift in convective cores, the very rapid uplift of air masses in tropical cyclones should be even more pronounced.

In summary, our trajectory calculations show that typhoons in the northern West Pacific have the potential to very rapidly uplift air masses from the sea surface up to altitudes of the Asian monsoon anticyclonic circulation within 1 to 2 days. Balloon measurements of water vapour and ozone in the Asian monsoon anticyclone launched in Kunming (China) in August 2009 show likewise a very rapid uplift of boundary sources associated with the typhoon Morakot and afterwards injection of these air masses in the Asian monsoon anticyclone (Munchak et al., 2010). These measurements support the results of our trajectory calculations for September 2012 showing that rapid uplift by typhoons in the West Pacific may transport air parcels from the boundary layer directly in the outer edge of the Asian monsoon anticyclone.

4.2 Asian monsoon anticyclone and eddy shedding in September 2012

In August 2012, the Asian monsoon anticyclone was well established over Southern Asia and the Middle East. During both August and September the Asian monsoon anticyclone was influenced by strong Rossby waves and by several tropical cyclones.

A time sequence of PV fields derived from ERA-Interim reanalysis data at 370 K potential temperature over Asia from 9 until 20 September 2012 is shown in Fig. 7 (colours) highlighting the fine-scale structure of PV in the anticyclone and the eastward propagation of filaments with low PV values at its northeastern flank (showing PV values < 5 PVU). In addition, the horizontal velocity (white arrows) characterising spatial and temporal evolution of the flow in the Asian monsoon anticyclone are shown.

On 9 September 2012, the Asian monsoon anticyclone ~~is~~ was located over South Asia and Northeast Africa (Fig. 7). At the northeastern flank of the anticyclone filaments with PV values lower than 5 PVU ~~evolve~~ evolved between 10–14 September. The filament with low PV ~~is~~ was extruded eastward along the subtropical westerly jet. A separation of the filament from the Asian monsoon circulation occurred and a small anticyclonic system developed during 15–16 September 2012. Thereafter, the secondary small anticyclone ~~is elongated, moves westward and merges with an other~~ was elongated, moved westward and merged with another newly formed filament on the eastern flank of the Asian monsoon with low PV values close to Japan on 17/18 September. On 20 September, again a secondary anticyclone, larger than the secondary anticyclone from 15/16 September, ~~is~~ was separated from the Asian monsoon anticyclone and ~~carries~~ carried air with low PV to the Pacific Ocean. Finally, the low PV air ~~moves~~ moved further eastwards along the subtropical jet across the extratropical tropopause to Northern Europe and ~~dissipates~~ dissipated slowly with time in the Northern Hemisphere lowermost stratosphere. ~~The~~

In September 2012, the subtropical jet was disturbed by strong Rossby waves triggered by low pressure systems travelling with the Arctic jet. The interaction between these disturbances and the subtropical jet can lead to baroclinic instabilities and eddy shedding (e. g. Orlanski and Sheldon, 1995) a process of peeling off secondary anticyclonic structures ~~is called eddy shedding event and occurs~~ occurring a few times each summer (Dethof et al., 1999; Hsu and Plumb, 2001; Popovic and Plumb, 2001) (cf. Sect. 1). Figure 7 shows that both the Asian monsoon anticyclone and the secondary eastward propagating anticyclones are characterised by low PV values, indicating that it consists mainly of air masses of tropospheric origin.

~~The general behaviour of 40day backward trajectories shown in Fig. 3 can be explained by the temporal evolution of the Asian monsoon anticyclone. Nearly all trajectories below a Θ_{org} of 380K are affected by the eddy shedding event on 20~~

~~September 2012 or by the separation of filaments with low PV values at the northeastern flank of the anticyclone.~~

4.3 ~~Reasons for eastward eddy shedding and intensification by a supertyphoon~~

~~suggested that mid-latitude synoptic disturbances occasionally interact with~~ Both the Asian monsoon anticyclone and ~~might pull filaments of tropospheric air from its northern flank. This process is referred to as eastward eddy shedding . Such a situation occurred in September 2012. The subtropical jet was disturbed by strong Rossby waves triggered by low pressure systems travelling with the Arctic jet. The interaction between these disturbances and the subtropical jet can lead to baroclinic instabilities and eddy shedding .~~

~~Under such circumstances, tropospheric air masses from the the Asian monsoon anticyclone are separated within a secondary anticyclone which is~~ the secondary eastward propagating anticyclone are still a tropospheric feature~~as indicated by low PV values~~. The transport of air masses into the lowermost stratosphere occurs afterwards. In contrast, tropospheric intrusions transport directly quasi-isentropically air masses from the tropical tropopause layer (TTL) into the extra-tropical lowermost stratosphere, where the air masses are mixed irreversibly (e.g., Vogel et al., 2011b). This can be caused by Rossby wave breaking events along the subtropical jet (e.g., Homeyer et al., 2011).

~~Moreover, the eddy shedding event of 20 September 2012 was intensified by interaction between the baroclinic waves and a super typhoon (class 5), leading to a weakening of the Asian monsoon anticyclone in its intensity and coherent horizontal structure.show that the impact of a tropical cyclone on the Rossby wave can be quantified as a source of wave activity for the upper-level wave and is sensitive to the phasing between the tropical cyclone and the wave. The interaction with the tropical cyclone can in general initiate wave breaking and, in case of the Asian monsoon anticyclone, lead to the shedding of secondary anticyclones from the main anticyclone.~~

~~On 10 September 2012,~~ Fig. 7 shows in addition the temporal movement of the super typhoon Sanba (PAGASA name Karen) ~~formed as a tropical depression east of the Philippines and started moving northward. Three days later the storm system underwent a strong intensification and evolved into~~ the strongest typhoon (class 5) during 2012 in the western Pacific region[4]~~(see Fig. 7)~~. It made landfall on 17 September in South Korea ~~and changed into an extratropical cyclone afterwards~~ (see Fig. 7) ~~.~~

~~A trough evolved upstream of the Himalayan plateau on 16 September 2012. This perturbation pushed the circulation~~ coincident with the process of peeling off secondary anticyclonic structures of the Asian monsoon anticyclone. Whether typhoon Sanba had an impact on the eddy shedding event of the Asian monsoon anticyclone ~~equatorwards and led to a split of the anticyclone in a western part centred over the Arabian peninsula and an eastern part over northern India. The western part weakened during the following days. At this stage the super typhoon Sanba approached the trough off the coast of South Korea (see~~ in September 2012, and whether this in a more general feature of typhoons, is an interesting open question, which requires further investigations.

The general behaviour of 40 day backward trajectories shown in Fig. ~~7). The subsequent interaction between the tropical typhoon and the baroclinic wave led to a strong amplification of the system. The typhoon acted as a source for eddy kinetic energy, leading to a strengthening of the meridional wind. The mid-latitude synoptic disturbances yield eastward eddy shedding strengthened by the super typhoon Sanba~~ 1 of the supplementary material and in Fig. 3 (main body of the paper) can be explained by the temporal evolution of the Asian monsoon anticyclone. The period between 10 and 20 September 2012 is very active in terms of release of filaments and eddy shedding events with two pronounced events on 14 and 20 September on the northeast flank of the Asian monsoon anticyclone (see Fig. 7) ~~.~~ causing the separation of the trajectories from the flow around the core of the anticyclone. Nearly all trajectories originating below 380 K show this separation between 10 and 20 September 2012.

In summary, our trajectory calculations show that typhoons in the northern west Pacific have the potential to very rapidly lift air masses from the sea surface to the edge of the Asian monsoon anticyclone within 1 to 2 days. In combination with the monsoon anticyclone and eastward eddy shedding events, this constitutes a new rapid transport pathway of surface emissions form the West Pacific to Northern Europe. In our study, the minimum transport times from surface to the lowermost stratosphere over Northern Europe are approximately 5 weeks. Moistening of the stratosphere is an important driver of climate change, therefore the role of this new rapid transport pathway in moistening of the extratropical lower stratosphere during summer needs further investigation.

Moreover, in the last 30 years a poleward migration occurred of the latitude where tropical cyclones achieve their lifetime-maximum intensity (Kossin et al., 2014). If this environmental change continues, more tropical cyclones migrate ~~polwards~~ polewards to the northeastern flank of the Asian monsoon anticyclone. Therefore, the frequency of occurrence of ~~both~~ the direct injections of polluted wet boundary layer air masses by very rapid uplift in typhoons into the Asian monsoon anticyclone ~~and the strength of eastward~~ could increase.

[4] see e.g., http://www.nasa.gov/mission_pages/hurricanes/archives/2012/h2012_Sanba.html

5 Discussion

5.1 Limitations of trajectory calculations

In general, trajectory calculations have limitations due to trajectory dispersion by errors through interpolation of the wind data to the air parcel positions at a specific time. Over the timescales in question, also mixing can be relevant. Backward trajectory calculations as performed in our study can diagnose the origin of air parcels measured during the research flight on 26 September 2012 over Northern Europe. To confirm whether the pathways identified in backward trajectories are robust, forward trajectories calculations starting at the origin of the air parcels are useful. To corroborate our finding that trajectories starting in Pacific typhoons, circulating around the Asian monsoon anticyclone, released by eddy shedding events ~~could increase.~~and are finally transported eastwards by the subtropical jet can reach the region of interest over Northern Europe during the TACTS measurements on 26 September 2012, we calculated forward trajectories starting within the typhoon Bolaven and Tembin between 22 and 26 August 2012 at noon. These calculations show that trajectories starting on 22 to 26 August from typhoon Tembin do not reach the region of interest. However trajectories starting at typhoon Bolaven on 22, 23, 24 and 25 August (12:00 UTC) reach the region of interest. Fig. 8 shows trajectories started at the typhoon Bolaven on 23 August at noon (see Sect. 4.1). Shown are only trajectories that reach the region of interest during the flight on 26 September 2012 12:00 UTC (at locations between 365 K and 385 K, between 55°N and 70°N, and between 20°W and 0°W). These calculations confirm that air masses from the typhoon Bolaven have the potential to reach the region of interest within ≈ 5 weeks. Our calculations show that trajectories based on wind fields from ERA-Interim reanalysis data experience rapid uplift in tropical cyclones and can reach the flightpath of the TACTS flight on 26 September 2012 in the lower stratosphere over Northern Europe. The coincidence of forward and backward trajectory analysis demonstrates that the transport pathways identified in our study are unaffected by limitations due to trajectory dispersion caused by interpolation processes. Further, the typhoon Bolaven could be identified as source of air masses from low levels of potential temperature.

5.2 Chemical contribution of air masses with different origins

All air parcels measured in the region of interest (except at the very beginning and end) are chemically affected by the troposphere, however only 5% of the backward trajectories originate in the troposphere (Θ_{org} <360 K) and 34% in the Asian monsoon anticyclone or UTLS (360 K < Θ_{org} < 380 K). The trajectories describe only advective transport, but in the real atmosphere in addition mixing processes occur. Therefore the region of interest is a mixture of air masses from the troposphere and the stratosphere which is reflected in different origins of the backward trajectories. To infer the relative contribution of the 2% air parcels lifted within the typhoon to the composition of the measured air parcels in the region of interest also mixing processes have to be taken into account. This is not possible with a pure trajectory study, here only the relative contributions of the trajectory origins can be determined.

Deduced from the number of trajectories originating in the lower troposphere or in the Asian monsoon anticyclone (5 % + 12 %), we conclude that in the region of interest a small amount air (17 %) with high concentrations of CO, CH_4, and H_2O is mixed with a huge amount of unpolluted dry stratospheric air (61 %). Filaments or eddy shedding events (see Fig. 7) transport polluted wet tropospheric air from the Asian monsoon into the lowermost stratosphere over Northern Europe. We assume that within these filaments or small anticyclones the tropospheric amount of trace gases is frozen in the core and only at the edge of the filaments/anticyclones mixing with stratospheric air occurred, therefore the tropospheric characteristic of these air masses can be transported over a large distance from Asia to Europe before the filaments dissipate slowly in the lowermost stratosphere. This kind of mixing process is described in more detail e. g. in Vogel et al. (2011b) in a case study analyzing the transport of a tropospheric intrusions from the tropical tropopause layer (TTL) into the lowermost stratosphere over mid and high latitudes.

5.3 Sixty days backward trajectories

A non-negligible fraction of the parcels (12%) in the region of interest (cf. Sect. 2) is also transported from the Asian monsoon region towards Northern Europe. In order to assess the geographical origin of these air parcels in the boundary layer, we calculated backward trajectories further beyond the 40 days limit. For that purpose, 60 days backward trajectories were calculated, a common trajectory length to study transport processes in the Asian monsoon region (ranging from a couple of weeks to a few months (e. g. Chen et al., 2012; Bergman et al., 2013).

For the region of interest, the origins of 60 days backward trajectories coming from low levels of potential temperature, from the Θ_{org} interval 285 K–320 K, are clustered in Southeast Asia, West Pacific Ocean, Bay of Bengal, and the Arabian Sea. 53 % of these trajectories from Θ_{org} values between 285 K and 320 K are from locations between 10°S, 40°N, 60°E, and 160°E. The origins of other trajectories are distributed in several different geographical regions (see Fig. 3 in the electronic supplement of this paper).

The origins of trajectories from higher levels of potential temperature, from the Θ_{org} interval 320 K–360 K, are

concentrated around the Tibetan Plateau, Northeast China, Mongolia, Southeast Asia, and the Pacific Ocean. 55 % of these trajectories from Θ_{org} values between 320 K and 360 K are from locations between 0°N, 50°N, 60°E, and 160°E. Also here, the origins of other trajectories are distributed globally (see Fig. 3 in the electronic supplement of this paper). Calculations of 60 day backward trajectories confirm that the origins of the air masses with enhanced values of tropospheric trace gases such as CH_4, CO, and H_2O found in the region of interest during the TACTS flight on 26 September 2012 are mainly due to boundary source emissions in Asia.

In Sect. 3, it is shown that in addition to the region of interest (cf. Sect. 2), in an other part of the flight enhanced tropospheric signals in tracers and reduced ozone are measured between 08:05 UTC and 08:23 UTC. However, in 40 day backward trajectories no evidence is found that these air masses are from lower levels of potential temperature. But calculations of 60 day backward trajectories show that also in this part of the flight, as well as in the region of interest, some of the trajectories originate at low levels of potential temperature between 295 K and 320 K. Fig. 9 shows that these air parcels are also from Southeast Asia and experience very rapid uplift on 2-3 August 2012 southeast of the Philippines. The reason for the strong upward transport is again a typhoon, namely typhoon 'Haikui'[5].

The results from 60 day backward trajectories demonstrate that very rapid uplift in typhoons in combination with the Asian monsoon anticyclone is not a single case of long-range transport, but rather a fast transport pathway from boundary layer in Asia to the lowermost stratosphere over Northern Europe that occurs more frequently. How frequently this pathway is expected to take place is an interesting open question. During the typhoon season 2012[6] 11 typhoons occurred between June and September. But also tropical depressions and tropical storms have the potential for very rapid uplift of boundary layer emissions. The impact of each of theses events in combination with the Asian monsoon anticyclone has to be analysed. We expect that the impact of this pathway is smaller compared to other (slower) transports from the tropical troposphere into the extratropical lower stratosphere. However, the impact of this rapid transport pathway is clearly evident in the TACTS measurements. The impact of this transport pathway also depends on the particular species considered. The shorter lived the species, the more important the fast transport pathway will be provided that the lifetime of the species is longer than the transport time.

[5] see e.g., http://www.nasa.gov/mission_pages/hurricanes/archives/2012/h2012_Damrey.html

[6] see e. g.:http://en.wikipedia.org/wiki/2012_Pacific_typhoon_season season summary

6 Conclusions

On 26 September 2012, a filament with enhanced tropospheric trace gases such as CH_4, CO, and H_2O and reduced stratospheric O_3 was measured over Northern Europe in the extratropical lowermost stratosphere during a flight on board the German Research Aircraft HALO during the TACTS campaign. Trajectory calculations show that these air masses originate in Southeast Asia and are affected by the Asian monsoon anticyclone. Based on our analysis of these observations and the associated trajectory calculations, we propose a new rapid transport pathway of approximately 5 weeks from the boundary layer sources in Southeast Asia to the location of the measurement in the lowermost stratosphere over Northern Europe.

Our findings show that air originating in the polluted boundary layer in South East Asia can be very rapidly lifted within 1–2 days by Pacific typhoons into air masses circulating around the Asian monsoon anticyclone (at ≈ 365 K potential temperature). Similar timescales are found for deep ~~convection~~ convective overshooting in this region (Chen et al., 2012) or in convective transport in the West African tropics (e.g., Fierli et al., 2011). Therefore, our findings confirm evidence from previous studies that at the eastern side of the anticyclone tropospheric air masses are lifted and trapped in the anticyclone (Li et al., 2005) or can be injected by convection into the stratosphere (Rosenlof et al., 1997; Park et al., 2007, 2008; Chen et al., 2012). Moreover, boundary emissions from ~~the core of~~ India or China lifted within the Asian monsoon anticyclone are not found in 40 day backward trajectories, but in 60 day backward trajectories suggesting that transport from boundary emissions from India and China through the Asian monsoon anticyclone is ~~slower~~comparatively slow.

However, we cannot rule out that a strong uplift in convection over India and Tibet is not well enough resolved in ERA-Interim reanalysis data in contrast to convection in tropical cyclones that are much larger than most convective cells. This might lead to a certain underestimation of upward transport in smaller scale convective systems compared to upward transport in typhoons.

In Fig. 10, selected 40 day backward trajectories representing characteristic pathways with different vertical velocities (cf. Table 1) are shown as ~~function~~ functions of potential temperature and longitude summarising our results. The figure illustrates different transport pathways of air masses with different ~~origin~~ origins to the location of the measurement over Northern Europe. The observed air masses in the region of interest are a mixture of air masses with distinct origins in different fractions (cf. Table 1). The combination of very rapid uplift by a typhoon and eastward eddy shedding from the Asian monsoon anticyclone yield fast transport (≈ 5 weeks) from Southeast Asia boundary layer sources to Northern Europe (2 % of all trajectories, red). Some of the 40 day backward trajectories originate in the West Pacific troposphere

(3 %, blue) or within the Asian monsoon anticyclone over South Asia/North Africa (12 %, green). Air masses that originate in the UTLS at altitudes between 370 K and 380 K potential temperature are mainly from the edge of the Asian monsoon anticyclone (22 %, yellow). Most air parcels originate at higher altitudes between 380 K and 420 K. These air parcels come from the entire Northern Hemisphere, with the exception of the region of the Asian monsoon anticyclone (61 %, grey).

Further, our calculations show that after the injection into the anticyclonic circulation, the air masses circulate clockwise, in an upward spiral, at the edge of the Asian monsoon anticyclone around the core of the anticyclone and do not enter the core of the anticyclone itself. In addition to the upward transport within the Asian monsoon connecting surface air with enhanced pollution to the lower stratosphere (e.g., Park et al., 2009; Randel et al., 2010; Chen et al., 2012; Bergman et al., 2013), the injection into the outer edge of the anticyclone and subsequent clockwise circulation around the core of the anticyclone is an additional pathway of air mass transport from the Asian monsoon anticyclone to the lowermost stratosphere. During the Nabro volcanic eruption in 2011, direct injections in the upper troposphere at the southwest flank of the Asian monsoon anticyclone (over Northwest Africa) have been observed by satellite observations by the Michelson Interferometer for Passive Atmospheric Sounding (MIPAS) (Griessbach et al., 2013). The MIPAS observations also show clockwise transport of air masses injected directly at the southwest flank in the outer edge of the Asian monsoon anticyclone. This support our findings about the clockwise transport of air masses injected directly at the east flank by typhoons around the core of the Asian monsoon anticyclone.

Our analysis shows that ~~an~~ eastward eddy shedding ~~event occurred mid of~~ events occurred in mid September 2012. The subtropical jet was disturbed by strong Rossby waves triggered by low pressure systems travelling with the Arctic jet. The interaction between these disturbances and the subtropical jet led to the peeling off of secondary anticyclonic structures from the Asian monsoon anticyclone. ~~In addition, this eddy shedding event was intensified by the interaction with the super typhoon Sanba.~~

The backward trajectories show that the transport time of water vapour and pollutants from the Asian monsoon anticyclone to Northern Europe caused by eddy shedding events and transport along the subtropical jet is about 8–14 days in the case study discussed here. Thereafter, the trajectories travel further northeastwards along the subtropical jet to the Pacific Ocean and finally to Northern Europe. In our study, moisture and pollution are transported very fast within up to 5 weeks from the lower troposphere in Southeast Asia to the lowermost stratosphere over Northern Europe caused by the combination of very rapid uplift by a typhoon and eastward eddy shedding from the Asian monsoon anticyclone. This rapid transport pathway into the lowermost stratosphere is for short-lived substances (e.g. bromine-containing very short-lived source gases) of particular importance. Eddy shedding events have the potential for long-range transport of enhanced concentrations of boundary layer sources such as water vapour and pollutants from Southeast Asia to mid and high latitudes of the Northern Hemisphere lowermost stratosphere.

Supplementary material related to this article is available online at: http://\@journalurl/\@pvol/\@fpage/\@pyear/\@journalnameshortlower-\@pvol-\@fpage-\@pyear-supplement.pdf.

Acknowledgements. We sincerely thank Andreas Engel and Harald Bönisch (University Frankfurt) for coordinating the TACTS campaign and the HALO crew and pilots for conducting the regarded flight. The authors gratefully acknowledge Paul Konopka and Felix Plöger (both at Research Centre Jülich) for helpful discussions ~~about~~ on the Asian monsoon circulation and Laura Pan ~~for discussions about~~ (NCAR, Boulder) for discussions on the balloon observations in China associated with the strong uplift in typhoons. We thank the European Centre of Medium-Range Weather Forcasts (ECMWF) for providing meteorological analyses and the ERA-Interim reanalysis data. Our activities, flight planning and forecasts were partly founded by the German Science Foundation (Deutsche Forschungsgemeinschaft, DFG) under the DFG project LASSO (HALO-SPP 1294/GR 3786). The authors thank three anonymous reviewers for their very helpful comments.

The service charges for this open access publication have been covered by a Research Centre of the Helmholtz Association.

References

references

Bannister, R. N., O'Neill, A., Gregory, A. R., and Nissen, K. M.: The role of the south-east Asian monsoon and other seasonal features in creating the "tape-recorder" signal in the Unified Model, Q. J. Roy. Meteor. Soc., 130, 1531–1554, 2004.

Bergman, J. W., Fierli, F., Jensen, E. J., Honomichl, S., and Pan, L. L.: Boundary layer sources for the Asian anticyclone: regional contributions to a vertical conduit, J. Geophys. Res., 118, 2560–2575, doi:http://dx.doi.org/10.1002/jgrd.5014210.1002/jgrd.50142, 2013.

Bourassa, A. E., Robock, A., Randel, W. J., Deshler, T., Rieger, L. A., Lloyd, N. D., Llewellyn, E. J. T., and Degenstein, D. A.: Large volcanic aerosol load in the stratosphere linked to Asian monsoon transport, Science, 337, 78–81, doi:http://dx.doi.org/10.1126/science.121937110.1126/science.1219371, 2012.

Chen, B., Xu, X. D., Yang, S., and Zhao, T. L.: Climatological perspectives of air transport from atmospheric boundary

layer to tropopause layer over Asian monsoon regions during boreal summer inferred from Lagrangian approach, Atmos. Chem. Phys., 12, 5827–5839, doi:http://dx.doi.org/10.5194/acp-12-5827-201210.5194/acp-12-5827-2012, 2012.

Dee, D. P., Uppala, S. M., Simmons, A. J., Berrisford, P., Poli, P., Kobayashi, S., Andrae, U., Balmaseda, M. A., Balsamo, G., Bauer, P., Bechtold, P., Beljaars, A. C. M., van de Berg, L., Bidlot, J., Bormann, N., Delsol, C., Dragani, R., Fuentes, M., Geer, A. J., Haimberger, L., Healy, S. B., Hersbach, H., Holm, E. V., Isaksen, L., Kallberg, P., Koehler, M., Matricardi, M., McNally, A. P., Monge-Sanz, B. M., Morcrette, J. J., Park, B.-K., Peubey, C., de Rosnay, P., Tavolato, C., Thepaut, J. N., and Vitart, F.: The ERA-Interim reanalysis: configuration and performance of the data assimilation system, Q. J. Roy. Meteor. Soc., 137, 553–597, doi:http://dx.doi.org/10.1002/qj.82810.1002/qj.828, 2011.

Dethof, A., O'Neill, A., Slingo, J. M., and Smit, H. G. J.: A mechanism for moistening the lower stratosphere involving the Asian summer monsoon, Q. J. Roy. Meteor. Soc., 556, 1079–1106, 1999.

Dunkerton, T. J.: Evidence of meridional motion in the summer lower stratosphere adjacent to monsoon regions, J. Geophys. Res., 100, 16675–16688, 1995.

Dvortsov, V. L. and Solomon, S.: Response of the stratospheric temperatures and ozone to past and future increases in stratospheric humidity, J. Geophys. Res., 106, 7505–7514, 2001.

Emanuel, K.: Tropical cyclons, Annu. Rev. Earth Pl. Sc., 3, 75–104, 2003.

Engel, A., Bönisch, H., Brunner, D., Fischer, H., Franke, H., Günther, G., Gurk, C., Hegglin, M., Hoor, P., Königstedt, R., Krebsbach, M., Maser, R., Parchatka, U., Peter, T., Schell, D., Schiller, C., Schmidt, U., Spelten, N., Szabo, T., Weers, U., Wernli, H., Wetter, T., and Wirth, V.: Highly resolved observations of trace gases in the lowermost stratosphere and upper troposphere from the Spurt project: an overview, Atmos. Chem. Phys., 6, 283–301, doi:http://dx.doi.org/10.5194/acp-6-283-200610.5194/acp-6-283-2006, 2006.

Fierli, F., Orlandi, E., Law, K. S., Cagnazzo, C., Cairo, F., Schiller, C., Borrmann, S., Di Donfrancesco, G., Ravegnani, F., and Volk, C. M.: Impact of deep convection in the tropical tropopause layer in West Africa: in-situ observations and mesoscale modelling, Atmos. Chem. Phys., 11, 201–214, doi:http://dx.doi.org/10.5194/acp-11-201-201110.5194/acp-11-201-2011, 2011.

Forster, P. and Shine, K. P.: Stratospheric water vapour change as possible contributor to observed stratospheric cooling, Geophys. Res. Lett., 26, 3309–3312, doi:http://dx.doi.org/10.1029/1999GL01048710.1029/1999GL010487, 1999.

Forster, P. and Shine, K. P.: Assessing the climate impact of trends in stratospheric water vapor, Geophys. Res. Lett., 29, 10-1–10-4 doi:http://dx.doi.org/10.1029/2001GL01390910.1029/2001GL013909, 2002.

Garny, H. and Randel, W. J.: Dynamic variability of the Asian monsoon anticyclone observed in potential vorticity and correlations with tracer distributions, J. Geophys. Res., 118, 13421–13433, doi:http://dx.doi.org/10.1002/2013JD02090810.1002/2013JD020908, 2013.

Gettelman, A., Kinnison, D., Dunkerton, T. J., and Brasseur, G. P.: Impact of monsoon circulations on the upper troposphere and lower stratosphere, J. Geophys. Res., 109, D22101, doi:http://dx.doi.org/10.1029/2004JD00487810.1029/2004JD004878, 2004.

Griessbach, S., Hoffmann, L., Spang, R., von Hobe, M., Müller, R., and Riese, M.: MIPAS Volcanic Sulfate Aerosol Observations of the Nabro Eruption, in: Stratospheric Sulfur and its Role in Climate (SSiRC), Atlanta, Georgia, USA, October 2013, SPARC, available at: http://www.sparc-ssirc.org/downloads/Griessbach.pdf, 2013.

Highwood, E. J. and Hoskins, B. J.: The tropical tropopause, Q. J. Roy. Meteor. Soc., 124, 1579–1604, 1998.

Holton, J. R., Haynes, P., McIntyre, M. E., Douglass, A. R., Rood, R. B., and Pfister, L.: Stratosphere–troposphere exchange, Rev. Geophys., 33, 403–439, 1995.

Homeyer, C. R., Bowman, K. P., Pan, L. L., Atlas, E. L., Gao, R.-S., and Campos, T. L.: Dynamical and chemical characteristics of tropospheric intrusions observed during START08, J. Geophys. Res., 116, D06111, doi:http://dx.doi.org/10.1029/2010JD01509810.1029/2010JD015098, 2011.

Hoor, P., Gurk, C., Brunner, D., Hegglin, M. I., Wernli, H., and Fischer, H.: Seasonality and extent of extratropical TST derived from in-situ CO measurements during SPURT, Atmos. Chem. Phys., 4, 1427–1442, doi:http://dx.doi.org/10.5194/acp-4-1427-200410.5194/acp-4-1427-2004, 2004.

Hsu, C. J. and Plumb, R. A.: Nonaxisymmetric thermally driven circulations and upper-tropospheric monsoon dynamics, J. Atmos. Sci., 57, 1255–1276, 2001.

Huang, Y., Zhang, W., Zheng, X., Li, J., and Yu, Y.: Modeling methane emission from rice paddies with various agricultural practices, J. Geophys. Res., 109, D8113, doi:http://dx.doi.org/10.1029/2003JD00440110.1029/2003JD004401, 2004.

Hurst, D. F., Oltmans, S. J., Vömel, H., Rosenlof, K. H., Davis, S. M., Ray, E. A., Hall, E. G., and Jordan, A. F.: Stratospheric water vapor trends over Boulder, Colorado: analysis of the 30 year Boulder record, J. Geophys. Res., 116, D02306, doi:http://dx.doi.org/10.1029/2010JD01506510.1029/2010JD015065, 2011.

Jackson, D. R., Driscoll, S. J., Highwood, E. J., Harries, J. E., and Russell III, J. M.: Troposphere to stratosphere transport at low latitudes as studies using HALOE observations of water vapor 1992–1997, Q. J. Roy. Meteor. Soc., 124, 169–192, 1998.

Kaufmann, M., Blank, J., Guggenmoser, T., Ungermann, J., Engel, A., Ern, M., Friedl-Vallon, F., Gerber, D.,, Grooß, J. U., Günther, G., Höpfner, M., Kleinert, A., Latzko, T., Maucher, G., Neubert, T., Nordmeyer, H., Oelhaf, H., Olschewski, F., Orphal, J., Preusse, P., Schlager, H., Schneider, H., Schuettemeyer, D., Stroh, F., Sumińska-Ebersoldt, O., Vogel, B., Volk, M., Wintel, J., Woiwode, W., and Riese, M.: Retrieval of three-dimensional small scale structures in upper tropospheric/lower stratospheric composition as measured by GLORIA, Atmos. Meas. Tech. Discuss., 7, 4229–4274, doi:http://dx.doi.org/10.5194/amtd-7-4229-201410.5194/amtd-7-4229-2014, 2014.

Khalil, M. A. K., Rasmussen, R. A., Shearer, M. J., Dalluge, R. W., Ren, L. X., and Duan, C. L.: Measurements of methane emissions

from rice fields in China, J. Geophys. Res., 103, 25181–25210, 1998.

Kirk-Davidoff, D. B., Hintsa, E. J., Anderson, J. G., and Keith, D. W.: The effect of climate change on ozone depletion through changes in stratospheric water vapour, Nature, 402, 399–401, doi:http://dx.doi.org/10.1038/4652110.1038/46521, 1999.

Konopka, P., Grooß, J.-U., Günther, G., Ploeger, F., Pommrich, R., Müller, R., and Livesey, N.: Annual cycle of ozone at and above the tropical tropopause: observations versus simulations with the Chemical Lagrangian Model of the Stratosphere (CLaMS), Atmos. Chem. Phys., 10, 121–132, doi:http://dx.doi.org/10.5194/acp-10-121-201010.5194/acp-10-121-2010, 2010.

Konopka, P., Ploeger, F., and Müller, R.: Entropy-based and static stability based Lagrangian model grids, in: Lagrangian Modeling of the Atmosphere, Geophysical Monograph Series, 200, AGU Chapman Conference on Advances in Lagrangian Modeling of the Atmosphere, Grindelwald, Switzerland, 9–14 October 2011, 99–109, 2012.

Kossin, J. P., Emanuel, K. A., and Vecchi, G. A.: The poleward migration of the location of tropical cyclone maximum intensity, Nature, 509, 349–352, doi:http://dx.doi.org/10.1038/nature1327810.1038/nature13278, 2014.

Kunz, A., Müller, R., Homonnai, V., Jánosi, I., Hurst, D., Rap, A., Forster, P., Rohrer, F., Spelten, N., and Riese, M.: Extending water vapor trend observations over Boulder into the tropopause region: trend uncertainties and resulting radiative forcing, J. Geophys. Res., 118, 11269–11284, doi:http://dx.doi.org/10.1002/jgrd.5083110.1002/jgrd.50831, 2013.

Li, Q., Jiang, J. H., Wu, D. L., Read, W. G., Livesey, N. J., Waters, J. W., Zhang, Y., Wang, B., Filipiak, M. J., Davis, C. P., Turquety, S., Wu, S., Park, R. J., Yantosca, R. M., and Jacob, D. J.: Convective outflow of South Asian pollution: a global CTM simulation compared with EOS MLS observations, Geophys. Res. Lett., 32, L14826, doi:http://dx.doi.org/10.1029/2005GL02276210.1029/2005GL022762, 2005.

Liu, Y., Wang, Y., Liu, X., Cai, Z., and Chance, K.: Tibetan middle tropospheric ozone minimum in June discovered from GOME observations, Geophys. Res. Lett., 36, L05814, doi:http://dx.doi.org/10.1029/2008GL03705610.1029/2008GL037056, 2009.

McKenna, D. S., Grooß, J.-U., Günther, G., Konopka, P., Müller, R., Carver, G., and Sasano, Y.: A new Chemical Lagrangian Model of the Stratosphere (CLaMS): 2. Formulation of chemistry scheme and initialization, J. Geophys. Res., 107, 4256, doi:http://dx.doi.org/10.1029/2000JD00011310.1029/2000JD000113, 2002a.

McKenna, D. S., Konopka, P., Grooß, J.-U., Günther, G., Müller, R., Spang, R., Offermann, D., and Orsolini, Y.: A new Chemical Lagrangian Model of the Stratosphere (CLaMS): 1. Formulation of advection and mixing, J. Geophys. Res., 107, 4309, doi:http://dx.doi.org/10.1029/2000JD00011410.1029/2000JD000114, 2002b.

Munchak, L., Fan, Q., Pan, L., Bian, J., and Bowman, K.: An analysis of transport pathways that contribute to water vapor and ozone profiles measured in the Asian monsoon anticyclone, in: Fall Meeting, Fall Meeting, 13–17 December 2010, AGU, San Francisco, A51B-0080, 2010.

Orlanski, I. and Sheldon, J. P.: Stages in the energetics of baroclinic systems, Tellus A, 47, 605–628, 1995.

Park, M., Randel, W. J., Kinnison, D. E., Garcia, R. R., and Choi, W.: Seasonal variation of methane, water vapor, and nitrogen oxides near the tropopause: Satellite observations and model simulations, J. Geophys. Res., 109, D03302, doi:http://dx.doi.org/10.1029/2003JD00370610.1029/2003JD003706, 2004.

Park, M., Randel, W. J., Gettleman, A., Massie, S. T., and Jiang, J. H.: Transport above the Asian summer monsoon anticyclone inferred from Aura Microwave Limb Sounder tracers, J. Geophys. Res., 112, D16309, doi:http://dx.doi.org/10.1029/2006JD00829410.1029/2006JD008294, 2007.

Park, M., Randel, W. J., Emmons, L. K., Bernath, P. F., Walker, K. A., and Boone, C. D.: Chemical isolation in the Asian monsoon anticyclone observed in Atmospheric Chemistry Experiment (ACE-FTS) data, Atmos. Chem. Phys., 8, 757–764, doi:http://dx.doi.org/10.5194/acp-8-757-200810.5194/acp-8-757-2008, 2008.

Park, M., Randel, W. J., Emmons, L. K., and Livesey, N. J.: Transport pathways of carbon monoxide in the Asian summer monsoon diagnosed from Model of Ozone and Related Tracers (MOZART), J. Geophys. Res., 114, D08303, doi:http://dx.doi.org/10.1029/2008JD01062110.1029/2008JD010621, 2009.

Ploeger, F., Konopka, P., Günther, G., Grooß, J.-U., and Müller, R.: Impact of the vertical velocity scheme on modeling transport across the tropical tropopause layer, J. Geophys. Res., 115, D03301, doi:http://dx.doi.org/10.1029/2009JD01202310.1029/2009JD012023, 2010.

Ploeger, F., Günther, G., Konopka, P., Fueglistaler, S., Müller, R., Hoppe, C., Kunz, A., Spang, R., Grooß, J.-U., and Riese, M.: Horizontal water vapor transport in the lower stratosphere from subtropics to high latitudes during boreal summer, J. Geophys. Res., 118, 8111–8127, doi:http://dx.doi.org/10.1002/jgrd.5063610.1002/jgrd.50636, 2013.

Pommrich, R., Müller, R., Grooß, J.-U., Konopka, P., Ploeger, P., Vogel, B., Tao, M., Hoppe, C., Günther, G., Hoffmann, L., Pumphrey, H.-C., Viciani, S., D'Amato, F., Volk, M., Hoor, P., Schlager, H, and Riese, M.: Tropical troposphere to stratosphere transport of carbon monoxide and long-lived trace species in the Chemical Lagrangian Model of the Stratosphere (CLaMS), Geosci. Model Dev. Discuss., 7, ~~submitted~~5087-5139, doi:http://dx.doi.org/10.5194/gmdd-7-5087-201410.5194/gmdd-7-5087-2014, 2014.

Popovic, J. M. and Plumb, R. A.: Eddy Shedding from the upper-tropospheric Asian monsoon anticyclone, J. Atmos. Sci., 58, 93–104, 2001.

Randel, W. J. and Park, M.: Deep convective influence on the Asian summer monsoon anticyclone and associated tracer variability observed with Atmospheric Infrared Sounder (AIRS), J. Geophys. Res., 111, D12314, doi:http://dx.doi.org/10.1029/2005JD00649010.1029/2005JD006490, 2006.

Randel, W. J., Park, M., Emmons, L., Kinnison, D., Bernath, P., Walker, K. A., Boone, C., and Pumphrey, H.: Asian monsoon transport of pollution to the stratosphere, Science, 328, 611–613, doi:http://dx.doi.org/10.1126/science.118227410.1126/science.1182274, 2010.

~~Riemer, M. and Jones, S. C.: Interaction of a tropical cyclone with a high-amplitude, midlatitude wave pattern: wavinessanalysis, trough deformation and track bifurcation, Q. J. Roy. Meteor. Soc., 140, 1362–1376, , 2013.~~

Riese, M., Grooß, J.-U., Feck, T., and Rohs, S.: Long-term changes of hydrogen-containing species in the stratosphere, J. Atmos. Sol-Terr. Phys., 68, 1973–1979, 2006.

Riese, M., Ploeger, F., Rap, A., Vogel, B., Konopka, P., Dameris, M., and Forster, P.: Impact of uncertainties in atmospheric mixing on simulated UTLS composition and related radiative effects, J. Geophys. Res., 117, D16305, doi:http://dx.doi.org/10.1029/2012JD01775110.1029/2012JD017751, 2012.

Riese, M., Oelhaf, H., Preusse, P., Blank, J., Ern, M., Friedl-Vallon, F., Fischer, H., Guggenmoser, T., Höpfner, M., Hoor, P., Kaufmann, M., Orphal, J., Plöger, F., Spang, R., Suminska-Ebersoldt, O., Ungermann, J., Vogel, B., and Woiwode, W.: Gimballed Limb Observer for Radiance Imaging of the Atmosphere (GLORIA) scientific objectives, Atmos. Meas. Tech., 7, 1915–1928, doi:10.5194/amt-7-1915-2014, 2014.

Röckmann, T., Grooß, J.-U., and Müller, R.: The impact of anthropogenic chlorine emissions, stratospheric ozone change and chemical feedbacks on stratospheric water, Atmos. Chem. Phys., 4, 693–699, doi:http://dx.doi.org/10.5194/acp-4-693-200410.5194/acp-4-693-2004, 2004.

Rohs, S., Schiller, C., Riese, M., Engel, A., Schmidt, U., Wetter, T., Levin, I., Nakazawa, T., and Aoki, S.: Long-term changes of methane and hydrogen in the stratosphere in the period 1978–2003 and their impact on the abundance of stratospheric water vapor, J. Geophys. Res., 111, D14315, doi:http://dx.doi.org/10.1029/2005JD00687710.1029/2005JD006877, 2006.

Rosenlof, K. H., Tuck, A. F., Kelly, K. K., Russell III, J. M., and McCormick, M. P.: Hemispheric asymmetries in the water vapor and inferences about transport in the lower stratosphere, J. Geophys. Res., 102, 13213–13234, 1997.

Schiller, C., Krämer, M., Afchine, A., Spelten, N., and Sitnikov, N.: The ice water content of Arctic, mid latitude and tropical cirrus, J. Geophys. Res., 113, D24208, doi:http://dx.doi.org/10.1029/2008JD01034210.1029/2008JD010342, 2008.

Shindell, D. T.: Climate and ozone response to increased stratospheric water vapor, Geophys. Res. Lett., 28, 1551–1554, doi:http://dx.doi.org/10.1029/1999GL01119710.1029/1999GL011197, 2001.

Smith, C. A., Haigh, J. D., and Toumi, R.: Radiative forcing due to trends in stratospheric water vapour, Geophys. Res. Lett., 28, 179–182, 2001.

Solomon, S., Rosenlof, K., Portmann, R., Daniel, J., Davis, S., Sanford, T., and Plattner, G.-K.: Contributions of stratospheric water vapor to decadal changes in the rate of global warming, Science, 327, 1219–1223, doi:http://dx.doi.org/10.1126/science.118248810.1126/science.1182488, 2010.

Vogel, B., Feck, T., and Grooß, J.-U.: Impact of stratospheric water vapor enhancements caused by CH_4 and H_2 increase on polar ozone loss, J. Geophys. Res., 116, D05301, doi:http://dx.doi.org/10.1029/2010JD01423410.1029/2010JD014234, 2011a.

Vogel, B., Pan, L. L., Konopka, P., Günther, G., Müller, R., Hall, W., Campos, T., Pollack, I., Weinheimer, A., Wei, J., Atlas, E. L., and Bowman, K. P.: Transport pathways and signatures of mixing in the extratropical tropopause region derived from Lagrangian model simulations, J. Geophys. Res., 116, D05306, doi:http://dx.doi.org/10.1029/2010JD01487610.1029/2010JD014876, 2011b.

Vogel, B., Feck, T., Grooß, J.-U., and Riese, M.: Impact of a possible future global hydrogen economy on Arctic stratospheric ozone loss, Energy Environ. Sci., 5, 6445–6452, doi:http://dx.doi.org/10.1039/c2ee03181g10.1039/c2ee03181g, 2012.

Xiong, X., Houweling, S., Wei, J., Maddy, E., Sun, F., and Barnet, C.: Methane plume over south Asia during the monsoon season: satellite observation and model simulation, Atmos. Chem. Phys., 9, 783–794, doi:http://dx.doi.org/10.5194/acp-9-783-200910.5194/acp-9-783-2009, 2009.

Zahn, A., Weppner, J., Widmann, H., Schlote-Holubek, K., Burger, B., Kühner, T., and Franke, H.: A fast and precise chemiluminescence ozone detector for eddy flux and airborne application, Atmos. Meas. Tech., 5, 363–375, doi:http://dx.doi.org/10.5194/amt-5-363-201210.5194/amt-5-363-2012, 2012.

Zöger, M., Schiller, C., and Eicke, N.: Fast in situ hygrometers: a new family of balloonborne and airborne Lyman-α photofragment fluorescence hygrometers, J. Geophys. Res., 104, 1807–1816, 1999.

Table 1. Number (N_{trajs}) and percentage of all trajectories in the region of interest (in total 432 trajectories), mean and maximum vertical velocity (calculated between 17 and 27 August 2012) along 40 day backward trajectories depending on levels of potential temperature at the air mass origin (Θ_{org}). The 40 day backward trajectories starting at the observation on 26 September 2012 and ending at the origin of the air masses in the past (17 August 2012). The air mass origins in terms of altitude and geographical position are also listed.
table

Θ_{org}	N_{trajs}	precentage	mean vertical velocity	max. vertical velocity	altitude origin	geographical position origin
295–320 K	8	2 %	very rapid uplift: 31 K day^{-1} (= 371 hPa day^{-1}) (= 6.6 km day^{-1}) 13 K/6 h (= 144 hPa/6 h) (= 2.5 km/6 h)	 41 K day^{-1} (= 523 hPa day^{-1}) (= 9.4 km day^{-1}) 21 K/6 h (= 276 hPa/6 h) (= 3.7 km/6 h)	boundary layer	Southeast Asia
320–360 K	15	3 %	rapid uplift: 8 K day^{-1} (= 63 hPa day^{-1}) (= 2.3 km day^{-1}) 3 K/6 h (= 31 hPa/6 h) (= 1.1 km/6 h)	 13 K day^{-1} (= 139 hPa day^{-1}) (= 4.4 km day^{-1}) 5 K/6 h (= 66 hPa/6 h) (= 1.9 km/6 h)	troposphere	mainly West Pacific
360–370 K	50	12 %	moderately rapid uplift: 2 K day^{-1} (= 22 hPa day^{-1}) (= 1.0 km day^{-1}) 1 K/6 h (= 11 hPa/6 h) (= 0.5 km/6 h)	 5 K day^{-1} (= 41 hPa day^{-1}) (= 1.8 km day^{-1}) 2 K/6 h (= 25 hPa/6 h) (= 1.1 km/6 h)	AM anticyclone	mainly South Asia/North Africa
370–380 K	97	22 %	moderate uplift: 1 K day^{-1} (= 16 hPa day^{-1}) (= 0.8 km day^{-1}) 0.5 K/6 h (= 8 hPa/6 h) (= 0.4 km/6 h)	 3 K day^{-1} (= 45 hPa day^{-1}) (= 2.3 km day^{-1}) 1 K/6 h (= 20 hPa/6 h) (= 1.0 km/6 h)	UTLS	mainly edge of the AM anticyclone
380–420 K	262	61 %	mainly descent		lower stratosphere	Northern Hemisphere

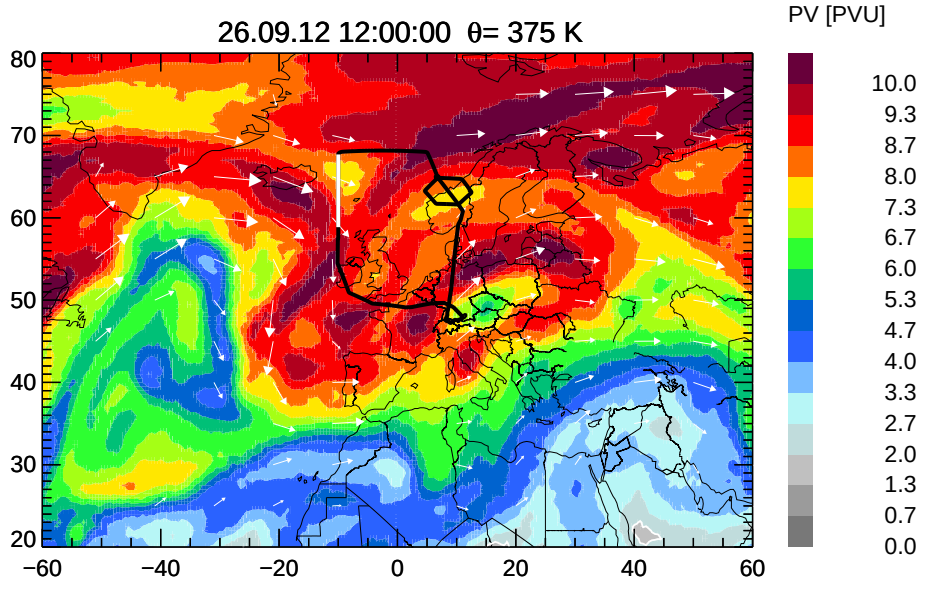

Fig. 1. The horizontal distribution of PV at 375 K potential temperature over Northern Europe on 26 September 2012. The flight path for the TACTS flight on 26 September 2012 (at flight time) starting and ending in Oberpfaffenhofen (near Munich, 48° N 11° E, Germany) is marked in black. The part of the flightpath discussed within this paper is highlighted in white (cf. Sect. 2 and see Fig. 2). The horizontal winds are indicated by white arrows. PV and horizontal winds are from ERA-Interim reanalysis data.
figure

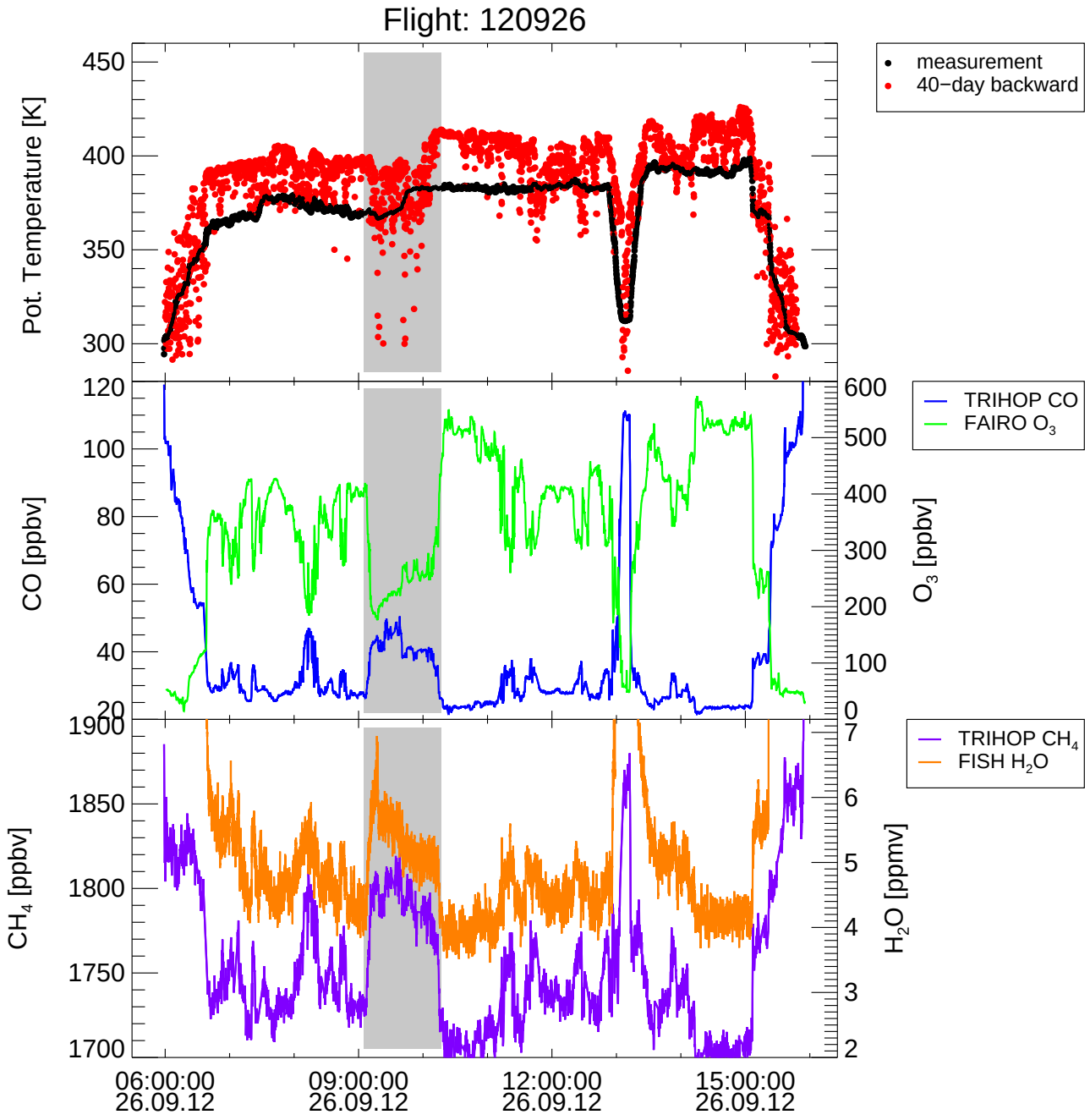

Fig. 2. Time evolution (given in Universal Time Coordinated (UTC~~time~~)) of potential temperature, CO, O_3, CH_4, and H_2O measurements for the flight on 26 September 2012. Potential temperature values at the end points of 40 day backward trajectories (17 August 2012) are shown as red dots (upper panel). The part of the flightpath discussed within this paper is highlighted in grey (region of interest) (cf. Sect. 2 and see Fig. 1). Trajectories with origins (Θ_{org}) lower than 360 K potential temperature in the region of interest are shown in Fig. 3.

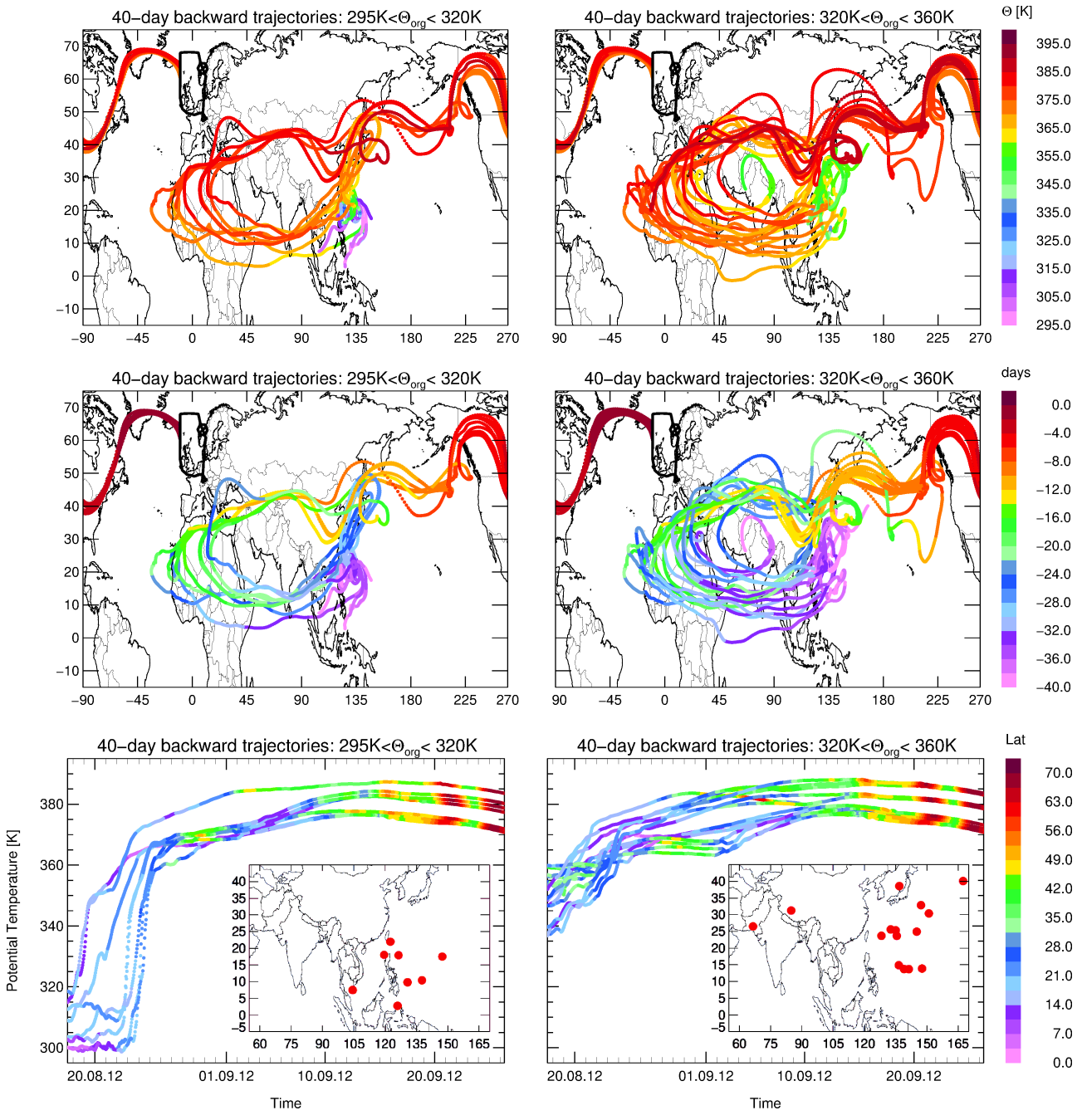

Fig. 3.

Fig. 3. Different 40 day backward trajectories for Θ_{org} intervals 295–320 K (left) and 320–360 K (right) are shown colour-coded by potential temperature (top) and by days reversed from 26 September 2012 (middle). Further, potential temperature vs. time (in UTC) along 40 day backward trajectories (bottom) are shown. Here, the colour indicate the latitude position of the trajectories. The trajectory positions are plotted every hour (coloured dots). Large distances between single dots indicated very rapid uplift. The geographical position of the origins (Θ_{org}) of the 40 day backward trajectories (red dots) are shown in the embedded longitude-latitude-cut. It should be noted that these geographical positions are at levels of potential temperature in the given Θ_{org} intervals and not at surface level.

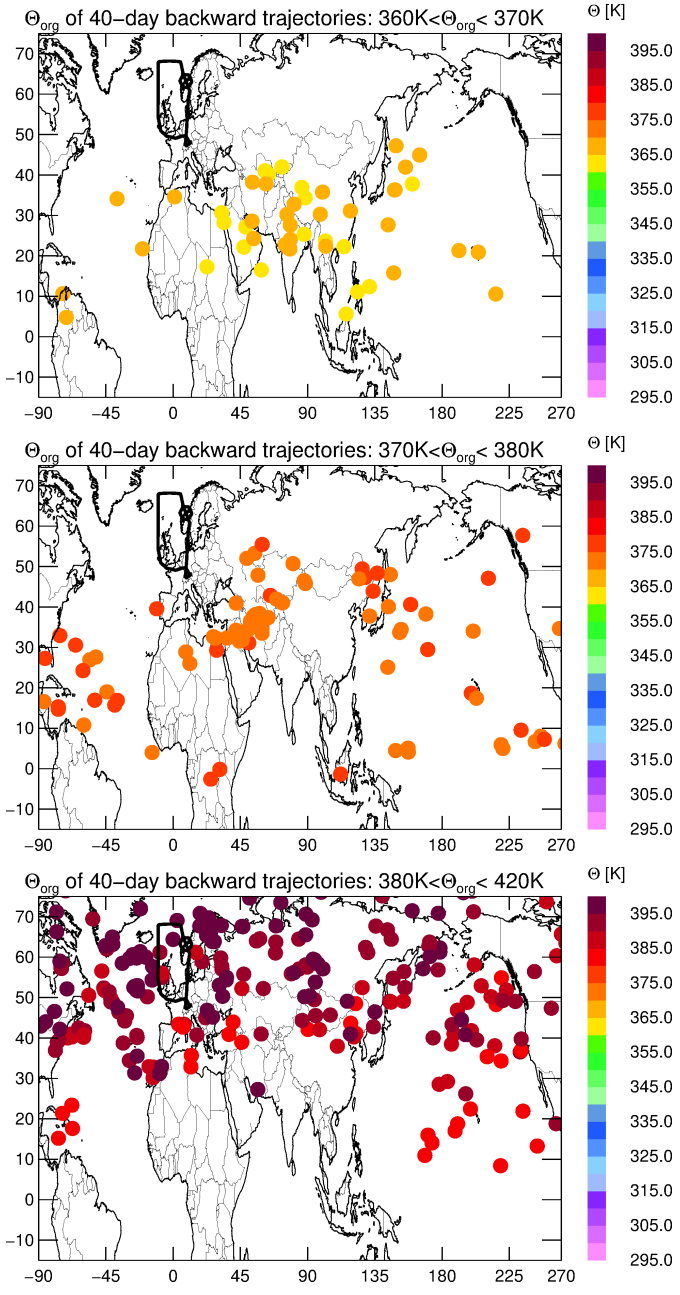

Fig. 4. The geographical position of the origins (Θ_{org}) of the 40 day backward trajectories for intervals 360–370 K (top), 370–380 K (middle) and 380–420 K (bottom) are shown colour-coded by potential temperature. The corresponding trajectories are shown in the electronic supplement of this paper.

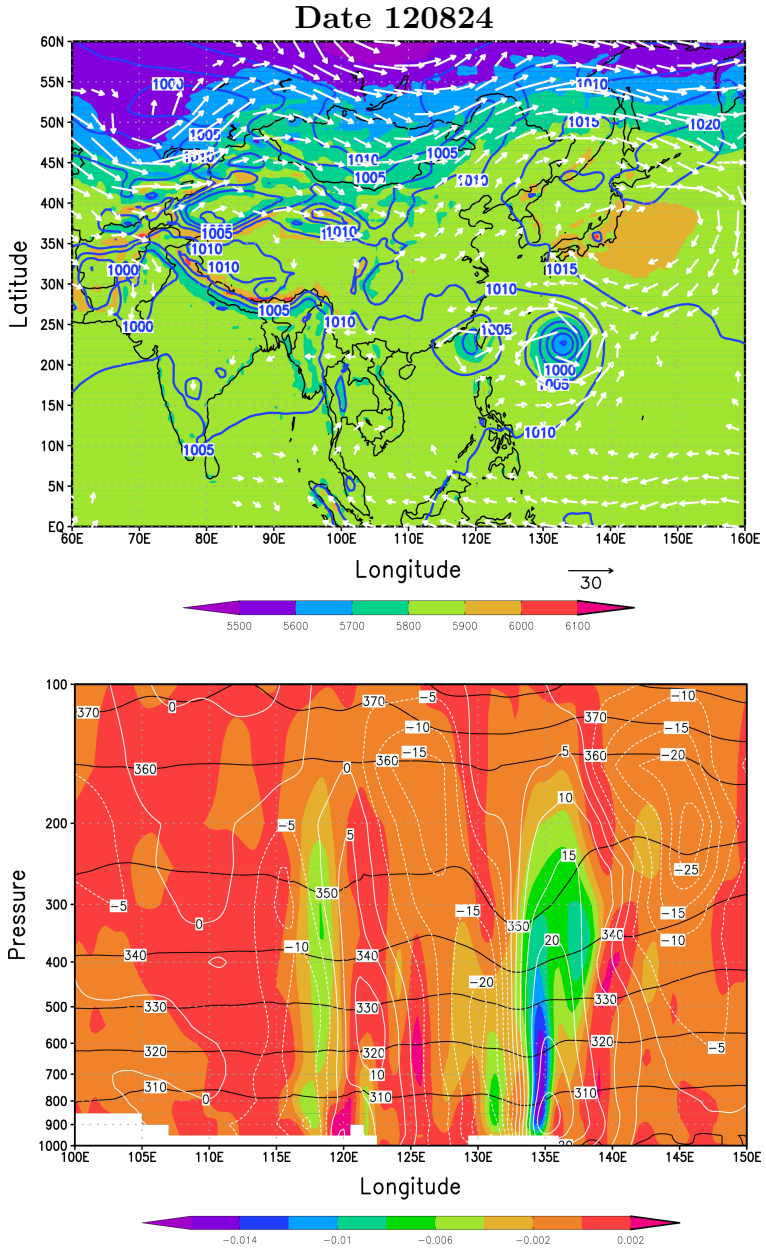

Fig. 5.

Fig. 5. Geopotential height in [m] (colour) and horizontal winds in $[\mathrm{ms}^{-1}]$ (white arrows) at 500 hPa on 24 August 2012 taken from ERA-Interim reanalysis data (top). To show the position of the typhoons Tembin ($\approx 23^\circ$ N 118° E) and Bolaven ($\approx 23^\circ$ N 135° E) the mean sea level pressure in [hPa] is shown as blue thick lines. Longitude-height cross-section showing the typhoon Tembin and Bolaven at 23° N (bottom). The vertical velocity (ω) in $[\mathrm{hPa\,s}^{-1}]$ (colour), the horizontal winds in $[\mathrm{ms}^{-1}]$ (white line (positive values) and white dashed line (negative values)), and potential temperature in Kelvin (black lines) are shown. Very rapid uplift up to $-0.014\,\mathrm{hPa\,s}^{-1}$ is found at the eastern flank of typhoon Bolaven ($\approx 135^\circ$ E) and up to $-0.006\,\mathrm{hPa\,s}^{-1}$ is found at western flank of typhoon Tembin ($\approx 118^\circ$ E).

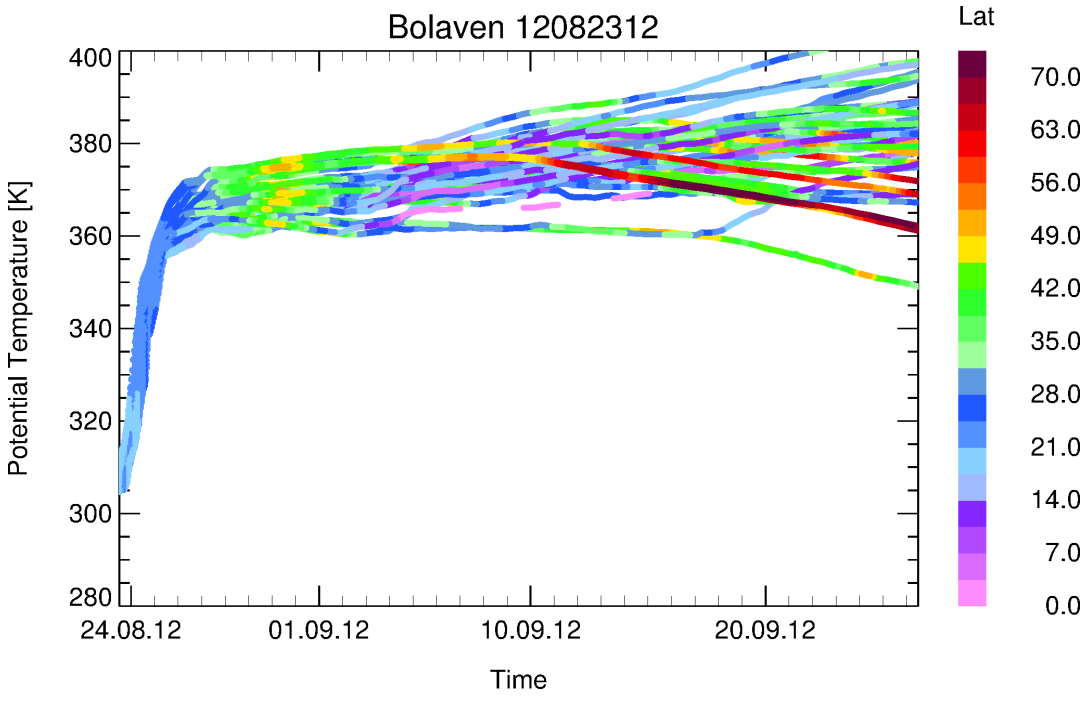

Fig. 6. Selected forward trajectories starting in the boundary layer around the position the typhoon Bolaven on 23 August 2012 12:00 UTC (15°N-25°N, 128°E-140°E and below ≈ 310 K potential temperature). The trajectories are started at a horizontal grid of 0.5° × 0.5° and a vertical grid of 1 K. Shown are only trajectories that experience a strong uplift greater than 50 K within the first 48 hours caused by typhoon Bolaven. For simplification only a subset of the trajectories is shown (every 100th trajectory).

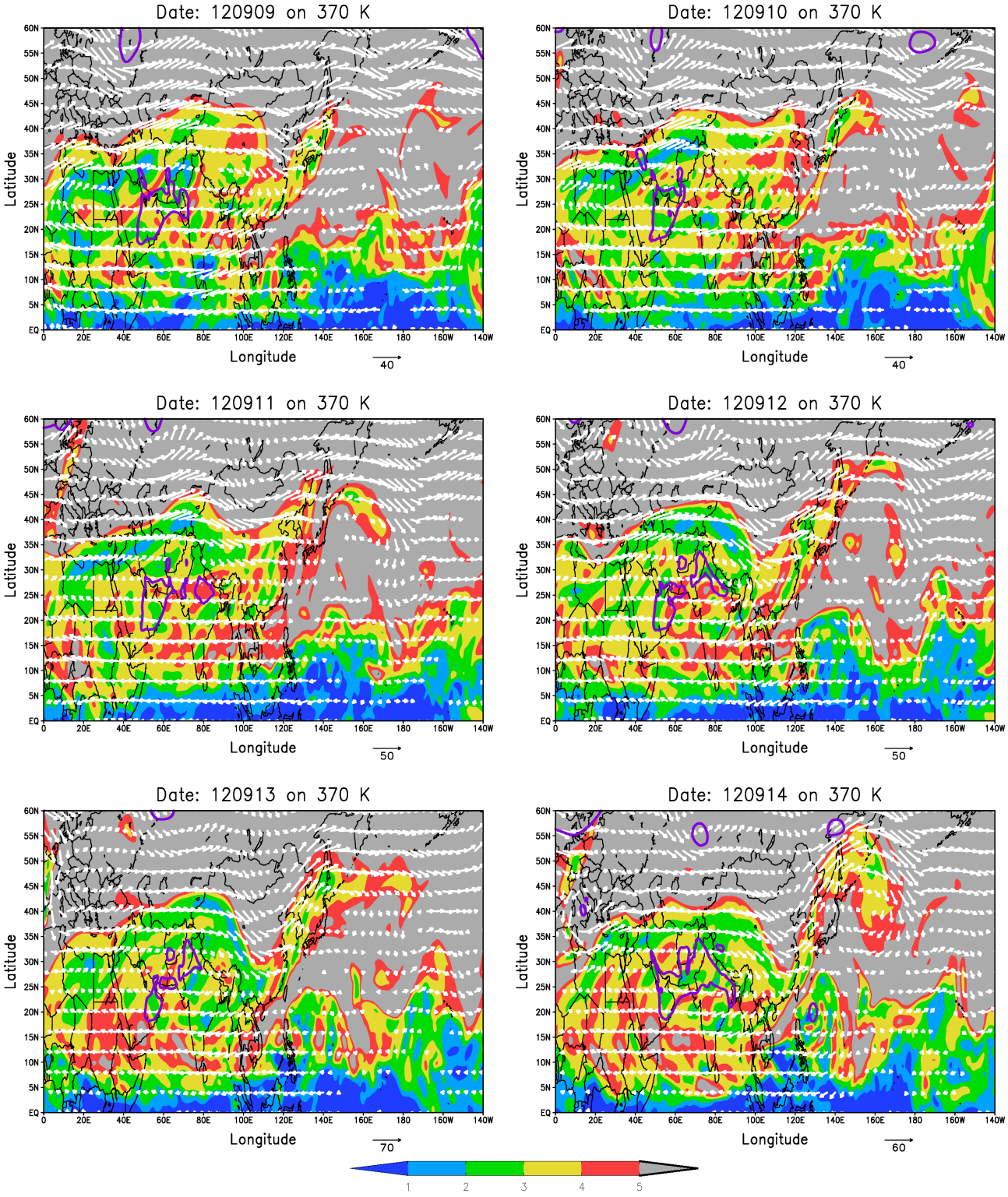

Fig. 7. Time sequence of PV fields (colour shading in PVU) over Asia at 370 K potential temperature from 9 to 20 September ~~2012.~~ 2012 based on ERA-Interim reanalysis data. The horizontal winds are indicated by white arrows. To show the position of tropospheric low-pressure systems in particular the super typhoon Sanba (e.g. $\approx 20^\circ$ N 130° E on 14 September, $\approx 25^\circ$ N 130° E on 15 September, $\approx 30^\circ$ N 130° E on 16 September, and $\approx 40^\circ$ N 130° E on 17 September) the sea level pressure of 1000 hPa is marked as thick purple line.

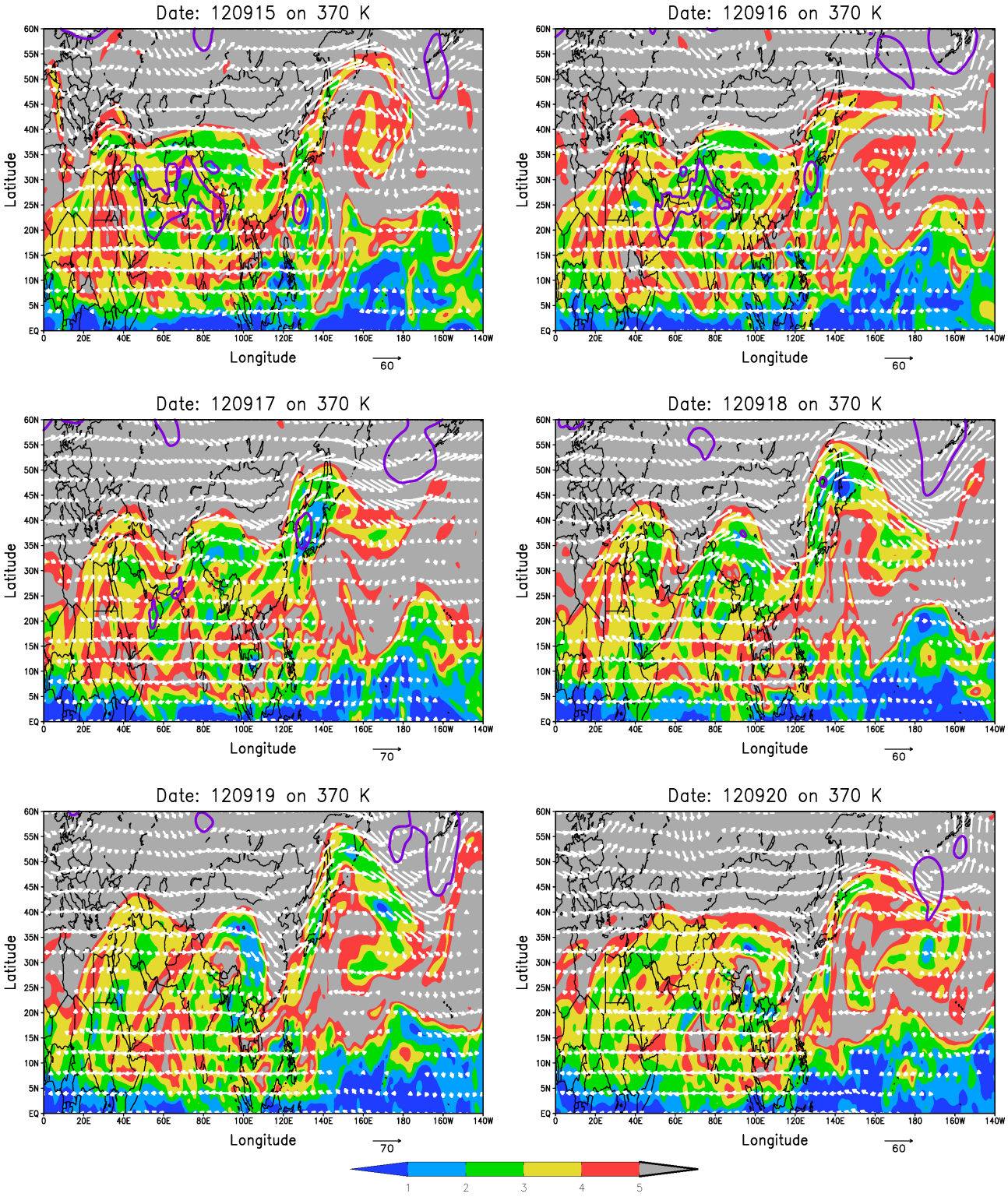

Fig. 7. Continued.

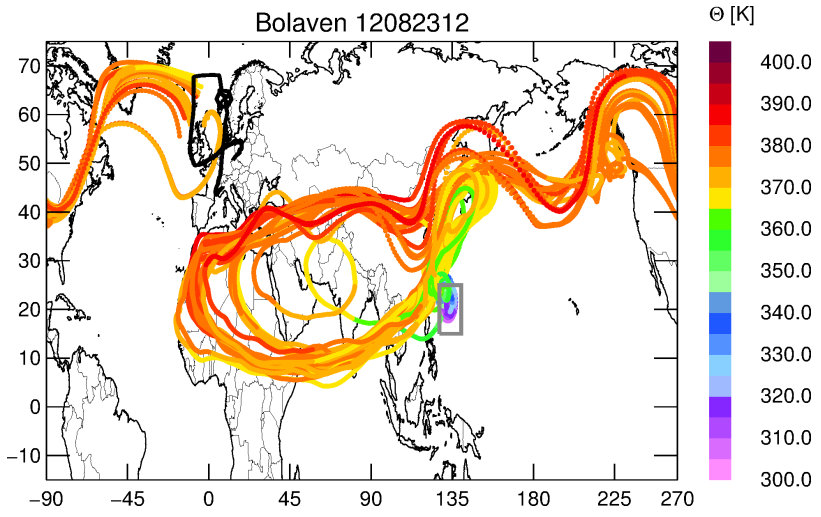

Fig. 8. Forward trajectories starting at the position of the typhoon Bolaven (15°N- 25°N, 128°E-140°E and below ≈ 310 K potential temperature) marked as grey box on 23 August 2012 12:00 UTC. Shown are only trajectories that reach the region of interest during the flight on 26 September 2012 12:00 UTC (at locations between 365 K and 385 K, between 55°N and 70°N, and between 20°W and 0°W). The flightpath shown in black is transformed to synoptic 12:00 UTC locations.

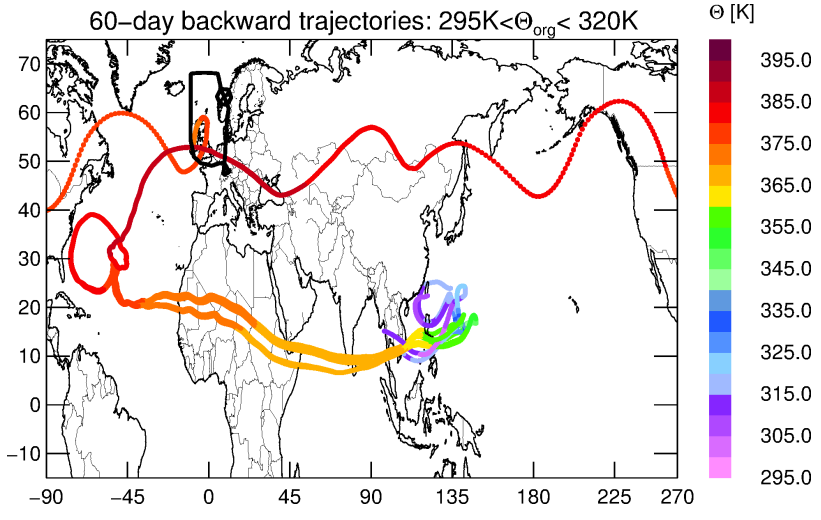

Fig. 9. Different 60 day backward trajectories for the tropospheric signal between 08:05 UTC and 08:23 UTC (see Fig. 2; enhanced values of CH_4, CO, and H_2O and reduced O_3 occurring before the region of interest) originating at low level of potential temperature (Θ_{org} = 295–320 K). The very rapid uplift over Southeast Asia is caused by typhoon Haikui.

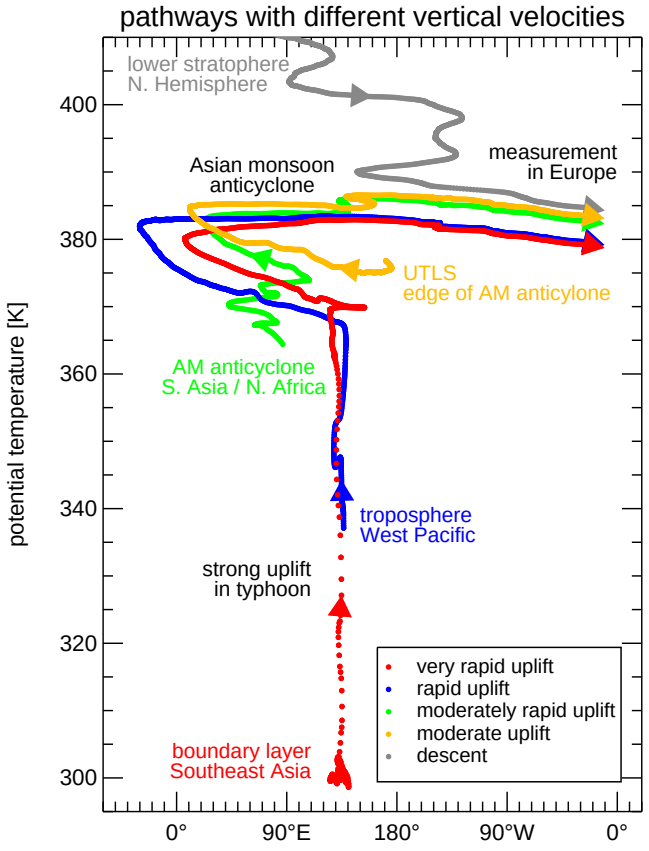

Fig. 10. Selected trajectories representing characteristic pathways with different vertical velocities (cf. Table 1) as function of potential temperature and longitude for the time period between 17 August and 26 September 2012. The air mass positions are plotted every hour (coloured dots). Large distances between the single dots indicated very rapid uplift. The classification of the different vertical velocities is derived for the first ten days of the trajectories (17–28 August 2012). For simplification longitudes between 60° W and 20° E are shown twice. The coloured text gives information about the altitude origin and geographical position origin of the different pathways. The figure illustrates different transport pathways of air masses with different origin to the location of the measurement over Northern Europe. The combination of very rapid uplift by a typhoon and eastward eddy shedding from the Asian monsoon anticyclone yield fast transport (≈ 5 weeks) from Southeast Asia boundary layer sources to Northern Europe (red).